THE JOURNAL OF PHYSICAL CHEMISTRY A

Article

Cite This: J. Phys. Chem. A 2019, 123, 10290−10302

pubs.acs.org/JPCA

Electronic Structure and Bonding of the Fastidious Species CN_2 and CP_2: A First-Principles Study

Aristotle Papakondylis* and Aristides Mavridis*

Department of Chemistry, Laboratory of Physical Chemistry, National and Kapodistrian University of Athens, Panepistimiopolis Zografou, Athens 157 71, Greece

ABSTRACT: The transient molecular species CN_2 (CNN, NCN, c(yclic)-CN_2) and CP_2 (CPP, PCP, c(yclic)-CP_2), along with the isoelectronic to CNN and isovalent to CPP, CCO, have been studied theoretically through the ab initio methodologies multireference configuration interaction (MRCI) and RCCSD(T) coupled with augmented correlation-consistent quintuple and sextuple basis sets. For the CNN, NCN, and c-CN_2 molecules, the examined states are [$\tilde{X}^3\Sigma^-$, $\tilde{a}^1\Delta$, $\tilde{b}^1\Sigma^+$, $\tilde{A}^3\Pi$, and $\tilde{c}^1\Pi$], $\tilde{X}^3\Sigma_g^-$, and $\tilde{X}^1A_1$, respectively. The analogous phosphorous system CPP has been studied theoretically for the first time. Our results show that the symmetries $^3\Sigma^-$, $^1\Delta$, and $^1\Sigma^+$ are not stationary states; thence, the ground state of CPP is of $^3\Pi$ symmetry and of similar electronic structure to that of the $\tilde{A}^3\Pi$ state of CNN. For most of the symmetries studied, we have constructed fully optimized potential energy profiles or "cuts" through the corresponding surfaces at the MRCI level of theory in an effort to follow the (valence) electronic distributions from the "selected" adiabatic species to equilibrium. Our numerical results are in excellent agreement with existing experimental data and previous, although limited, high-level ab initio calculations. Finally, it should be said that some of our findings like dissociation energies, permanent electric dipole moments, and bonding considerations are addressed for the first time.

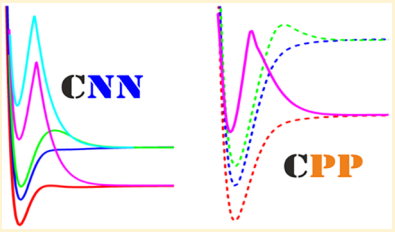

1. INTRODUCTION

The diazocarbene (CNN) molecule has been observed for the first time in 1960 by Robinson and McCarthy through irradiation of diazomethane (CH_2N_2) in krypton matrices at 4.2 K;[1] see also ref 2. In 1965, the CNN molecule was characterized as a linear triplet by electron paramagnetic resonance in frozen matrices at 4 K.[3] More than 10 years later Bondybey and English,[4] using vibrational spectroscopy in argon matrices, established that the ground state of CNN is $^3\Sigma^-$ locating as well the $\tilde{A}^3\Pi$ excited state at T_0 = 23 597 cm^{-1}; see also ref 5. It is fair to mention here that the ground-state symmetry of CNN, $^3\Sigma^-$, was predicted for the first time theoretically by Thomson in 1973 through an ab initio SCF/DZ + P (Slater basis set) study.[6]

Since 1965, the fascinating story of CNN unfolded in a long series of experimental[3−5,7−15] and ab initio theoretical studies.[6,13,15−25] Details on the experimental and theoretical work on CNN are summarized nicely by Wurfel et al.[12] (1992), Clifford et al.[13] (1998), Yamaguchi and Schaefer[21] (2004), Carter et al.[23] (2008), and Ornellas and co-workers[24] (2010) and therefore there is no need to be told again.

Table 1 collects the "best" or more recent pertinent experimental structural results of the first four ($\tilde{X}^3\Sigma^-$, $\tilde{a}^1\Delta$, $\tilde{b}^1\Sigma^+$, $\tilde{A}^3\Pi$) states of CNN, where our interest will be mainly focused. See also the remarkable compilation of experimental data by Jacox for about 1700 neutral and ionic transient molecules.[26] Concerning the CNN species, besides the first four states, data for two more triplets are also listed, i.e., the $\tilde{B}^3\Sigma^-$(?) and $\tilde{C}^3\Pi$(?) in the Jacox article.[26] However, common experimental structural results like equilibrium bond distances, r_e(C−N_2) and r_e(CN−N), or electrical dipole moments, μ_e, are missing from the literature for all (experimentally) investigated states of CNN, due rather to technical difficulties of handling this system.

As far as we know, the most recent high-level "standard" ab initio electronic structure theoretical works on CNN were presented by Yamaguchi and Schaefer in 2004[21] and Ornellas and co-workers in 2010.[24] Yamaguchi and Schaefer examined around equilibrium the $\tilde{X}^3\Sigma^-$ and $\tilde{A}^3\Pi$ states of CNN using the coupled-cluster (CC) approach in conjunction with a series of increasing sized basis sets, the largest being the quadruple correlation-consistent basis set cc-pVQZ of Dunning.[27] They report geometries, harmonic fundamental vibrational frequencies, electric dipole moments, the $\tilde{A}^3\Pi \leftarrow \tilde{X}^3\Sigma^-$ excitation energy, and the Renner−Teller splitting parameter ε of the $\tilde{A}^3\Pi$ state.[21] Ornellas et al.[24] investigated 16 states of CNN and the ground states of its ions CNN^+ and CNN^- using the [internally contracted (ic)] multireference configuration interaction (MRCI) and/or CC methods, combined with a series of increasing cardinality augmented correlation-consistent basis sets,[27] aug-cc-pV*n*Z (aV*n*Z, *n* = D, T, Q, 5), thus reporting results at the complete basis set ($CBS_{T\text{-}5}$) limit. They also examined the effect of including the six ~$1s^2$ core electrons for certain properties and states.[24] More specifically, the three states $\tilde{X}^3\Sigma^-$, $\tilde{a}^1\Delta$, and $\tilde{A}^3\Pi$ have been examined at the MRCI+Q/$CBS_{T\text{-}5}$ level (+Q refers to the Davidson correction), whereas for four more states, namely, $\tilde{b}^1\Sigma^+$, $\tilde{c}^1\Pi$, $\tilde{d}^1\Sigma^-$,

Received: September 25, 2019
Revised: October 29, 2019
Published: October 31, 2019

DOI: 10.1021/acs.jpca.9b09084
J. Phys. Chem. A 2019, 123, 10290−10302

Table 1. Existing Experimental Data for the First Four States of the CNN Radical[f]

state	$\omega_1(\sigma^+)$ (cm^{-1})	$\omega_2(\pi)$ (cm^{-1})	$\omega_3(\sigma^+)$ (cm^{-1})	T_0 (cm^{-1})	$D_0°$ (kcal/mol)	EA (eV)	A (cm^{-1})	ε
$\tilde{X}^3\Sigma^-$	1230 ± 120[a]	390 ± 120[a]	1425 ± 120[a]	0.0	35.3 ± 5[a]	1.771 ± 0.010		
	1235[b]	396[b]	1419[b]		28.1 ± 1.15[c]			
$\tilde{a}^1\Delta$			1600 ± 120[a]	6830 ± 120[a]				
$\tilde{b}^1\Sigma^+$				10 690 ± 120[a]				
$\tilde{A}^3\Pi$	1386[c]	525 ± 2[d]	1807 ± 2[d]	23 850[c]			−26.5[e]	−0.07[e]

[a]Ref 13. Gas phase photoelectron spectroscopy. [b]Ref 12. Laser-induced fluorescence spectroscopy in Ar matrices. [c]Ref 14. Gas phase photodissociation dynamics. [d]Ref 4. Laser fluorescence spectroscopy in Ar matrices. [e]Ref 11. Laser-induced fluorescence spectroscopy. [f]Fundamental vibrational frequencies ω [$\omega_1(\sigma^+)$, $\omega_2(\pi)$, $\omega_3(\sigma^+)$], excitation energies T_0, dissociation energy $D_0°$ (C−N_2), and electron affinity (EA) of the $\tilde{X}^3\Sigma^-$ state, and the spin−orbit parameter A and the Renner−Teller splitting ε of the $\tilde{A}^3\Pi$ state.

and $\tilde{B}^3\Sigma^-$, they give certain results at the MRCI+Q/aVTZ level. For the two first triplets $\tilde{X}^3\Sigma^-$ and $\tilde{A}^3\Pi$, the CCSD(T)/$CBS_{T\text{-}5}$ method was also applied, while vertical excitation energies are given at the MRCI+Q/$CBS_{T\text{-}5}$ level of theory for a series of excited states; see Table 4 of ref 24. Notice, however, that all calculations have been performed around equilibrium. Their results[24] as well as those by Yamaguchi and Schafer[21] will be compared with ours in due course. On the collisional dynamics of the C(^{1}D) + N_2($X^1\Sigma_g^+$) process, two very recent papers should be mentioned, that is, the first in 2016 by Hickson et al.[15] (experiment and theory) and the 2019 theoretical study by Guo and co-workers.[25]

Although the experimental and theoretical literature on CNN is quite extensive,[1−26] the literature on the phosphorous analogue of CNN carbon diphosphide, CPP, is scarce. Indeed, for the CP_2 species, isovalent to CN_2, we are aware of only two experimental papers published almost half a century ago.[28,29] A theoretical study on PCP published in 2000 will be considered later on. Both studies refer to gas phase Knudsen mass spectroscopy for a series of carbon−phosphorous molecules. Concerning CP_2, Smoes et al. say the following: "For CP_2, the atomization energy obtained is $\Delta H_{0,at}°$ (CP_2) = 963 ± 15 or 980 ± 15 kJ mol^{-1} for the alternate structures CPP or PCP, respectively",[28] and then, "It is thus likely that the molecule CP_2 observed is a mixture of both isomers". On the other hand, Kordis and Gingerich appear to be rather certain that they observe the isomer CPP by giving only one atomization energy of 231.9 ± 4.6 kcal mol^{-1},[29] essentially the same as the results of ref 28, 230.2 ± 3.6 or 234.2 ± 3.6 kcal/mol.

It should be mentioned though that our highly correlated ab initio calculations, while confirming essentially the numerical results of refs 28 and 29, preclude the CPP isomer. Our findings indicate that the stable isomer of the CP_2 species examined by these workers is the centrosymmetrical diradical PCP (but see below).

The four states $^3\Sigma^-$, $^1\Delta$, $^1\Sigma^+$, and $^3\Pi$ of the triatomic radicals CNN and CPP, as well as the $^1\Pi$ state of CNN, the third companion of the singlets, have been investigated by high-level multireference (MRCI) and coupled-cluster methods. The ground centrosymmetric diradical state of CN_2, NCN, has been also examined at both MRCI and RCCSD(T) levels of theory. It should be stressed that one of the purposes of the present work is to clarify, if possible, the bonding mechanisms of these unusual molecular systems. This is the reason that, in addition to CN_2, we also studied the $\tilde{X}^3\Sigma^-$ state of CCO, isoelectronic to CNN. Bonding in chemistry is of paramount importance, and the only way of being rationalized to a certain degree is through the ab initio tackling of the Schrödinger equation. For both systems, CN_2 and CP_2, we report geometries, harmonic fundamental vibrational frequencies, permanent electric dipole moments, energetics, full potential energy profiles (PEP), and thereby reasonable binding scenarios.

The present study is structured as follows: Section 2, labeled "Physical Insights", is a qualitative bonding description of the $^3\Sigma^-$ states of CN_2 (CNN and NCN) and CCO, which is surmised through valence-bond-Lewis (vbL) diagrams. It is followed by Section 3 on computational details. Results and discussion on the linear molecules CNN, NCN, and CPP, PCP are presented in Sections 4.1, 4.2, and 4.4, respectively, while the $\tilde{X}^1A_1$ state of the cyclic isomers of CN_2 (c-CN_2) and CP_2 (c-CP_2) is considered in Sections 4.3 and 4.5. Finally Section 5 epitomizes our results.

2. PHYSICAL INSIGHTS

The formation of the diazocarbene (CNN) radical in its lowest $^3\Sigma^-$ state can be thought as the linear approach of either N(^{4}S) to CN($X^2\Sigma^+$) from the N-side of the latter or in a similar fashion C(^{3}P) to N_2($X^1\Sigma_g^+$). Scheme 1 shows the two paths through the valence-bond-Lewis (vbL) diagrams (a) and (b), respectively.

Scheme 1. vbL Diagrams of the Interactions (a) CN($X^2\Sigma^+$) + N(^{4}S) and (b) C(^{3}P; M_L = 0) + N_2($X^1\Sigma_g^+$)

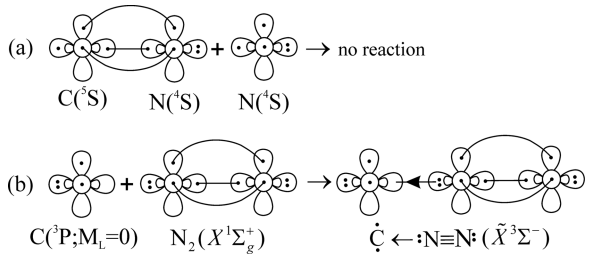

Notwithstanding the fact that the reactants of path (b), C + N_2, are about 77 mE_h (=48 kcal/mol) lower in energy than the corresponding species of (a), CN + N, the latter is precluded for evident reasons. Path (b) on the other hand, is a possible mechanism of the CNN formation, conforming as well to certain experimental results: CNN is linear ($C_{\infty v}$) and has a $^3\Sigma^-$ ground state and a weak C−N_2 bond dissociation energy of about 28 kcal/mol (see Table 1), as one would expect for a $\dot{C} \leftarrow :N_2$ harpoon-like bond. Note, however, that the vbL picture of Scheme 1b also suggests that both electrons coupled into a triplet are localized on the carbon atom and that the C−NN and CN−N bonds are of "single" and "triple" characters, respectively, while a modest increase of the CN−N "triple" bond as compared to the bond length of the free N_2($X^1\Sigma_g^+$) is expected due to the implied C ← N_2 charge transfer.

DOI: 10.1021/acs.jpca.9b09084
J. Phys. Chem. A 2019, 123, 10290−10302

Nevertheless, our calculations concerning the bonding mechanism of the $\tilde{X}^3\Sigma^-$ state of CNN should be interpreted with care (see below).

We would like now to discuss the cyanonitrene radical, NCN, the centrosymmetric isomer of CNN whose ground state $\tilde{X}^3\Sigma_g^-$ ($D_{\infty h}$) has been established experimentally; see the extended compilation by Jacox on the experimental literature of NCN.[26] The most natural way of realizing the NCN molecule is the approach of a nitrogen atom $N(^4S)$ from infinity to the cyano radical $CN(X^2\Sigma^+)$ from its C-end in a linear fashion. The vbL diagram of Scheme 2 depicts the expected result.

Scheme 2. vbL Diagram of NCN

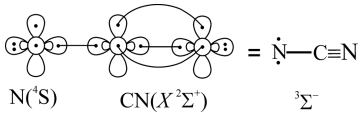

Quantum mechanics, however, requires the identity of the in situ left and right N atoms (no symmetry breaking), i.e., symmetry forces us to write down the following vbL diagram as to the electronic structure of NCN (Scheme 3). It is clear from

Scheme 3. vbL Diagram of NCN($\tilde{X}^3\Sigma_g^-$) after "Symmetrization"

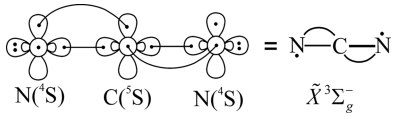

the vbL diagrams of Schemes 2 and 3 that the in situ C atom in $NCN(\tilde{X}^3\Sigma_g^-)$, and of course in $CN(X\ ^2\Sigma^+)$, is in the third excited ^5S state, 4.18 eV (=96.4 kcal/mol) above its ^3P ground state. Alternatively, the symmetric linear approach of two $N(^4S)$ atoms to a $C(^5S)$ atom leads to a $^3\Sigma_g^-$ state of NCN. Our calculations on the $\tilde{X}^3\Sigma_g^-$ state completely support the above centrosymmetric equilibrium structure imposed by symmetry (vide infra).

For a better understanding of the unusual electronic structure of CNN, it is instructive to consider the isoelectronic ketenylidene radical CCO. Recall that $CO(X^1\Sigma^+)$ is isoelectronic to $N_2(X^1\Sigma_g^+)$ and that both species carry "similar" electronic properties.[30] Experimental results on five CCO states ($\tilde{X}^3\Sigma^-$, $\tilde{a}^1\Delta$, $\tilde{b}^1\Sigma^+$, $\tilde{A}^3\Pi$, and $\tilde{c}^1\Pi$) can be found in the Jacox compilation,[26] whereas the story from its first observation by Jacox and her co-workers is told nicely by Brown, Yamaguchi, and Schaefer.[31] We are only interested in the $\tilde{X}^3\Sigma^-$ state of CCO as contrasted to the $\tilde{X}^3\Sigma^-$ state of CNN. Thinking along the same lines as before (see Scheme 2), the electronic structure of $CCO(\tilde{X}^3\Sigma^-)$ can be captured by the vbL diagram shown in Scheme 4.

Scheme 4. vbL Diagram of the Interaction of $C(^3P;\ M_L = 0)$ + $CO(X^1\Sigma^+)$

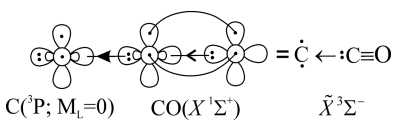

This "acid(Ċ)–base(:CO)" diagram clearly suggests the following as to the electronic structure of CCO: (a) the two electrons coupled into a triplet are localized on the first C atom, (b) a modest elongation of the CC–O equilibrium bond length as compared to the "triple" bond length of the free $CO(X\ ^1\Sigma^+)$, and (c) a relatively high electric dipole moment. Both (b) and (c) inferences are due to the Ċ ← :CO charge transfer. In addition, Scheme 4 suggests that the potential energy function of the reaction $C(^3P) + CO(X\ ^1\Sigma^+) \rightarrow CCO(\tilde{X}^3\Sigma^-)$ can be faithfully obtained even at the Hartree–Fock level and certainly at the single reference RCCSD(T) level. Our calculations are in agreement with the above anticipations, confirming the vbL diagram of Scheme 4, making clear that there are bonding differences between the $\tilde{X}^3\Sigma^-$ stationary states of CNN and CCO.

The carbon diphosphide radical CP_2 (CPP and PCP) isovalent to CN_2 (CNN and NCN) and CCO will be presented in Section 4. Suffice to say at this point that the CPP entity is investigated through ab initio calculations for the first time with rather unexpected results (see below).

3. COMPUTATIONAL DETAILS

The augmented polarized valence correlation-consistent basis sets of quintuple cardinality aug-cc-pV5Z (=a5Z) by Dunning and co-workers have been used for the C, N, and O atoms,[27,32] as well as for the P atom.[33] The a6Z basis set[32] was used only for the $\tilde{X}^3\Sigma^-$ and $\tilde{A}^3\Pi$ states of CNN around equilibrium. The a5Z basis sets employed for the CN_2 (CNN and NCN), CCO, and CP_2 (CPP and PCP) molecules were generally contracted in the usual way.

$$CN_2,\ CCO:\ (15s9p5d4f3g2h)_{C,N,O} \rightarrow [7s6p5d4f3g2h]_{C,N,O}$$

$$CP_2:\ (15s9p5d4f3g2h/_C 21s13p5d4f3g2h/_P) \rightarrow [7s6p5d4f3g2h/_C 8s7p5d4f3g2h/_P]$$

The corresponding a6Z contraction for the CNN molecule is

$$CNN:\ (17s11p6d5f4g3h2i)_{C,N} \rightarrow [8s7p6d5f4g3h2i]_{C,N}$$

spanning a space of spherical Gaussians of order 567. The a5Z basis set was also used for the brief examination of the cyclic isomers of CN_2 and CP_2, c-CN_2 and c-CP_2, respectively.

Two general computational routes were taken in the present work: the complete active space self-consistent field (CASSCF) + single + double replacement (CASCF + 1 + 2 = MRCI) method and the restricted (open) coupled-cluster + singles + doubles + quasiperturbative connected triples [RCCSD(T)].[34−36] The present report is addressed to seven molecular systems, i.e., $CNN(\tilde{X}^3\Sigma^-, \tilde{a}^1\Delta, \tilde{b}^1\Sigma^+, \tilde{A}^3\Pi, \tilde{c}^1\Pi)$, $NCN(\tilde{X}^3\Sigma_g^-)$, $CCO(\tilde{X}^3\Sigma^-)$, $CPP(^3\Sigma^-, {}^1\Delta, {}^1\Sigma^+, {}^3\Pi)$, and $PCP(\tilde{X}^3\Sigma_g^-)$ and the two cyclic "carbenes" c-CN_2 and c-CP_2 both of $^1A_1$ symmetry, whose CASSCF wave functions have been constructed by allotting 14 valence electrons to 12 orbitals. Subsequent internally contracted (ic)[37,38] MRCI wave functions were obtained through single and double replacements out of the CASSCF reference space. Core correlation effects were not taken into account, meaning that the ~1s (C, N, O) and ~1s2s2p (P) orbitals were kept always doubly occupied. The state-averaged technique with equal weights was applied for the two singlets $^1\Delta$ and $^1\Sigma^+$. All calculations were done under C_{2v} symmetry restrictions and when needed relaxed to C_s symmetry conditions. Fundamental harmonic

DOI: 10.1021/acs.jpca.9b09084
J. Phys. Chem. A 2019, 123, 10290–10302

Table 2. Total Energies E (E_h), Bond Distances r_e (Å), Dissociation Energies D_e and D_0 (kcal/mol), Harmonic Frequencies ω_e (cm^{-1}),[a] Electric Dipole Moments μ_e (D), and Excitation Energies T_e (T_0) (cm^{-1}) of the Ground $\tilde{X}^3\Sigma^-$ and the excited $\tilde{a}^1\Delta$, $\tilde{b}^1\Sigma^+$, $\tilde{A}^3\Pi$, $\tilde{c}^1\Pi$ States of CNN at the MRCI/a5Z and RCCSD(T)/a5Z,a6Z Levels[o]

method	−E	r_e(C−N)	r_e(N−N)	D_e[b]	D_0[b]	$\omega_1(\sigma^+)$, $\omega_2(\pi)$, $\omega_3(\sigma^+)$	μ_e[c]	T_e (T_0)
					$\tilde{X}^3\Sigma^-$			
MRCI	147.22408	1.2366	1.2041	30.9	29.0	1258, 426, 1602	0.88	0.0
MRCI+Q	147.2537	1.238	1.206	32.6	30.7		0.82	0.0
RCCSD(T)/a5Z	147.25411	1.2367	1.2008	31.7	30.2	1207, 403, 1359	0.76	0.0
RCCSD(T)/a6Z	147.25768	1.2364	1.2004	31.8	30.3			0.0
CCSD(T)/QZ[d]	147.242519	1.2372	1.2045			1253, 405, 1442	0.80	0.0
MRCI+Q/$CBS_{T\text{-}5}$[e]	147.260346	1.2363	1.2024		31.1	1254, 394, 1451		0.0
expt.					28.1 ± 1.15[f]	1235,[g] 396,[g] 1419[g]		0.0
					$\tilde{a}^1\Delta$			
MRCI	147.19241	1.2607	1.1823	41.3	38.8	1266, 455, 1907	0.63	6951 (7137)
MRCI+Q	147.2238	1.262	1.184	42.6	40.1		0.60	6554 (6740)
MRCI+Q/$CBS_{T\text{-}5}$[e]	147.229096	1.2603	1.1818					6965
expt.[h]						−, −, 1600 ± 120		(6830 ± 120)
					$\tilde{b}^1\Sigma^+$			
MRCI	147.17603	1.2729	1.1756	30.8	28.7	1222, 440, 1744	0.43	10 546 (10 613)
MRCI+Q	147.2067	1.274	1.177	31.7	29.6		0.40	10 315 (10 382)
MRCI+Q/$CBS_{T\text{-}5}$[e]	147.210186[i]	1.2716[j]	1.1794[j]					11 009[i]
expt.[h]								(10 690 ± 120)
					$\tilde{A}^3\Pi$			
MRCI	147.11708	1.2230	1.1815	−36.0	−38.9	1358, 526$^+$/603$^-$, 1896	−2.09	23 484 (23 800)
MRCI+Q	147.1464	1.224	1.183	−34.9	−37.8		−2.06	23 550 (23 866)
RCCSD(T)/a5Z	147.14548	1.2215	1.1795	−36.5	−39.3	1365, 513$^+$/612$^-$, 1818	−2.06	23 842 (24 177)
RCCSD(T)/a6Z	147.14913	1.2218	1.1792	−36.2	−39.0		−2.07	23 824 (24 159)
CCSD(T)/QZ[d]	147.132815	1.2232	1.1804			1359, 525,[k] 1848	2.06	23 960 (24 336)[l]
MRCI+Q/$CBS_{T\text{-}5}$[e]	147.151638	1.2227	1.1807			1358, 511$^+$/606$^-$, 1840		24 074
expt.						1386,[f] 525 ± 2,[m] 1807 ± 2[m]		(≈23 850)[f]
					$\tilde{c}^1\Pi$			
MRCI	147.07492	1.1823	1.2545	−32.6	−35.3	1128, 512/571, 2058[n]	−2.80	32 737 (33 015)
MRCI+Q	147.1060	1.185	1.255	−31.1	−33.8		−2.76	32 408 (32 686)

[a] $\omega_1(\sigma^+$; symmetric stretch), $\omega_2(\pi$; bend), $\omega_3(\sigma^+$; antisymmetric stretch). [b] Dissociation energy of the $\tilde{X}^3\Sigma^-$ and $\tilde{A}^3\Pi$ states with respect to $C(^3P)$ + $N_2(X^1\Sigma_g^+)$ and of the $\tilde{a}^1\Delta$, $\tilde{b}^1\Sigma^+$, and $\tilde{c}^1\Pi$ states with respect to $C(^1D)$ + $N_2(X^1\Sigma_g^+)$. [c] Permanent electric dipole moments have been obtained through the finite field approach; field strength, 7×10^{-5} au. [d] Ref 21. [e] Ref 24. Complete basis set limit of MRCI+Q/aTZ → MRCI+Q/a5Z. [f] Ref 14 and Table 1. [g] Ref 12 and Table 1. [h] Ref 13 and Table 1. [i] Obtained at the MRCI+Q/$CBS_{T\text{-}5}$ level. [j] Obtained at the MRCI+Q/aTZ level. [k] Ref 21. $\omega(\pi^+)/\omega(\pi^-)$ = 585/661 cm^{-1} at the cc-pVQZ EOM-CCSD level. [l] Ref 21. T_e based on CCSD/QZ//CCSDT-3/QZ and frequencies on CCSD(T)/QZ. [m] Ref 4 and Table 1. [n] Harmonic frequencies obtained at the MRCI/aug-cc-pVTZ level. [o] "Best" theoretical and experimental results from the literature are also included for comparison.

vibrational frequencies were calculated by diagonalizing the corresponding Hessian matrices calculated by numerical differentiation and using average atomic masses. As an indication of the magnitude of the present calculations, the CASSCF, MRCI, and icMRCI wave functions of the $\tilde{X}^3\Sigma^-$ state of CNN at equilibrium contain 70 746, 19.6×10^9, and 59.5×10^6 configuration functions (CFs), respectively. Of course, all our "MRCI" results refer to icMRCI wave functions. Finally, to mitigate nonextensivity errors, the Davidson correction (+Q) was applied.[39,40] At this level of theory and for the purpose of the present work, the basis set superposition error(s) or other type of corrections like core effects or basis set incompleteness are deemed as unnecessary.

All calculations were performed with the MOLPRO2015 suite of codes.[41]

4. RESULTS AND DISCUSSION

4.1. CNN. Table 2 collects all our numerical results on the five examined stationary states of the CNN radical, namely, $\tilde{X}^3\Sigma^-$, $\tilde{a}^1\Delta$, $\tilde{b}^1\Sigma^+$, $\tilde{A}^3\Pi$, and $\tilde{c}^1\Pi$ in ascending energy order along with the "best" ab initio results of the literature as well as relevant experimental data. Bear in mind that till now the experimental geometry of CNN and CCO is not known; the same holds true for their permanent electric dipole moments. With the exception of the (harmonic) vibrational frequencies, which can be considered in fair agreement with the experiment, our results are in excellent agreement with the experiment and recent ab initio results from the literature. For a definitive work on the fundamental vibrational frequencies of the $\tilde{X}^3\Sigma^-$ state of CNN, see ref 23. Figure 1 shows full, completely optimized MRCI potential energy profiles (PEP) or "cuts" through the potential energy surfaces of all five examined states of CNN, whereas Figure 2 displays the corresponding PEP of the $\tilde{X}^3\Sigma^-$ state of CCO at the RCCSD(T) level. In what follows, the pair of triplets ($\tilde{X}^3\Sigma^-$, $\tilde{A}^3\Pi$) is discussed first followed by the three singlets ($\tilde{a}^1\Delta$, $\tilde{b}^1\Sigma^+$, $\tilde{c}^1\Pi$), with the triplets correlating adiabatically to $C(^3P)$ + $N_2(X^1\Sigma_g^+)$ and the singlets to $C(^1D)$ + $N_2(X^1\Sigma_g^+)$. Along with the $\tilde{X}^3\Sigma^-$ state of CNN, we also refer to the $\tilde{X}^3\Sigma^-$ state of CCO just to contrast the bonding character of two very "similar" and isoelectronic molecules; even their molecular weights are identical. Numerical results for the $\tilde{X}^3\Sigma^-$ state of CCO are given in the second part of Table 3.

DOI: 10.1021/acs.jpca.9b09084
J. Phys. Chem. A 2019, 123, 10290−10302

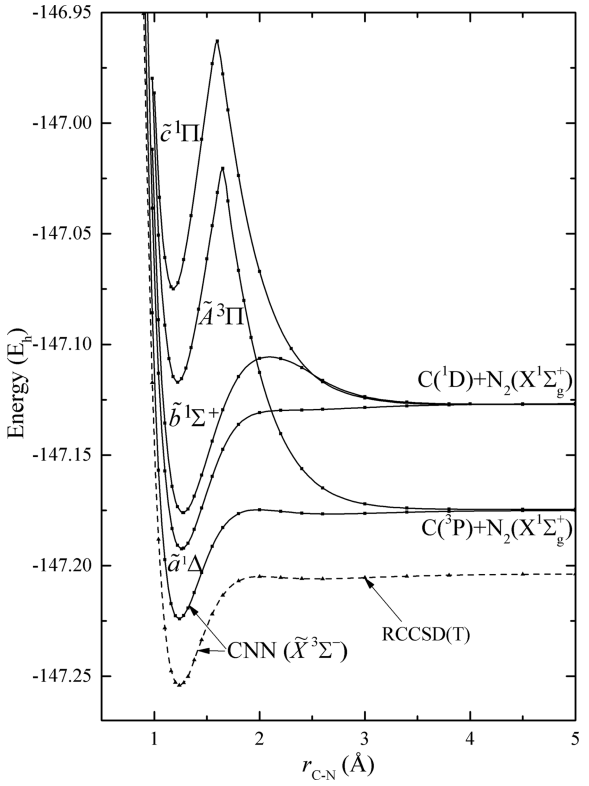

Figure 1. Fully optimized potential energy profiles for the collinear approaches $C(^3P) + N_2(X^1\Sigma_g^+)$ and $C(^1D) + N_2(X^1\Sigma_g^+)$ at the MRCI/a5Z level of theory. The RCCSD(T)/a5Z profile is also shown (dashed line) for the ground state of CNN.

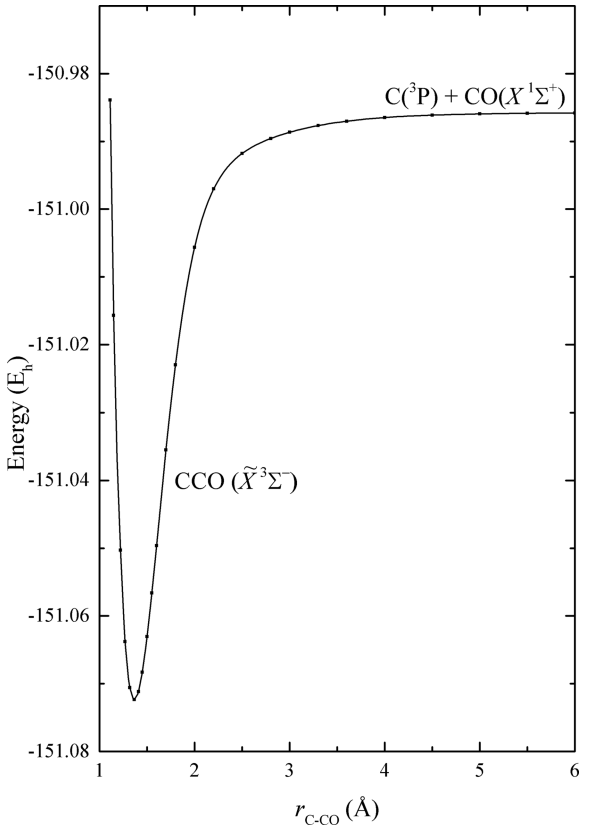

Figure 2. Potential energy profile for the collinear approach $C(^3P) + CO(X^1\Sigma^+)$ at the RCCSD(T)/a5Z level of theory.

4.1.1. $\tilde{X}^3\Sigma^-$, $\tilde{A}^3\Pi$. Recall that the core electrons, 6 for the CN_2 and CCO species ($\sim 1s^2/_{N,C,O}$) and 22 for the isovalent CP_2 system ($1s^2/_C\ 1s^2 2s^2 2p^6/_P$), were kept doubly occupied in all our post-Hartree−Fock calculations. On including them in the $\tilde{X}^3\Sigma^-$ and $\tilde{A}^3\Pi$ states of the CNN molecule at the UCCSD(T)/$CBS_{T\text{-}5}$ level, bond distances changed by less than a mere 0.001 Å (see Table 2 of ref 24).

The leading equilibrium MRCI configuration functions of the $\tilde{X}^3\Sigma^-$ states of CNN and CCO and their atomic Mulliken distributions are

$$CN_{(a)}N_{(b)}$$

$$|\tilde{X}^3\Sigma^-\rangle \approx 0.90|(\text{core})^6 4\sigma^2 5\sigma^2 6\sigma^2 7\sigma^2 1\pi^4 2\pi^2\rangle$$

$$2s^{1.64}2p_z^{0.96}2p_x^{0.65}2p_y^{0.65}/_C 2s^{1.30}2p_z^{1.06}2p_x^{1.27}2p_y^{1.27}/_{N(a)} 2s^{1.95}2p_z^{1.13}2p_x^{1.06}2p_y^{1.06}/_{N(b)}$$

$$C_{(a)}C_{(b)}O$$

$$|\tilde{X}^3\Sigma^-\rangle \approx 0.92|(\text{core})^6 4\sigma^2 5\sigma^2 6\sigma^2 7\sigma^2 1\pi^4 2\pi^2\rangle$$

$$2s^{1.88}2p_z^{1.02}2p_x^{0.68}2p_y^{0.68}/_{C(a)} 2s^{0.95}2p_z^{0.83}2p_x^{0.86}2p_y^{0.86}/_{C(b)} 2s^{1.86}2p_z^{1.44}2p_x^{1.47}2p_y^{1.47}/_O$$

where (core) = $1\sigma^2 2\sigma^2 3\sigma^2$ and $+0.10/_C$ $+0.10/_{N(a)}$ $-0.20/_{N(b)}$ and $-0.26/_{C(a)}$ $+0.50/_{C(b)}$ $-0.24/_O$ are net Mulliken charges of CNN and CCO, respectively. At all levels of theory, equilibrium bond distances are in excellent agreement with previous high-level calculations,[21,24] with our "best" RCCSD(T)/a6Z numbers being r_e(C−NN) = 1.2364 and r_e(CN−N) = 1.2004 Å (Table 2). The experimental dissociation energy, D_0° = 28.1 ± 1.15 kcal/mol,[14] is in harmony at all levels of theory MRCI(MRCI+Q)[RCCSD(T)/a6Z], D_0° = 29.0(30.7)[30.3] kcal/mol, in practical agreement with the MRCI+Q/$CBS_{T\text{-}5}$ D_0° = 31.1 kcal/mol of ref 24. Finally, the RCCSD(T)/a5Z finite field dipole moment is μ_e = 0.76 D (Table 2).

What about the bonding, however, of the $\tilde{X}^3\Sigma^-$ state of CNN? The CN−N equilibrium bond distance of 1.2004 Å is larger by 0.10 Å than that of the free N_2 ($r_e(X^1\Sigma_g^+)$ = 1.0977 Å[30]), pointing to a "double" CN−N bond and raising questions as to the validity of the mechanism suggested by Scheme 1b. Figure 1 shows the fully optimized potential energy profile of the $C(^3P) + N_2(X^1\Sigma_g^+)$ interaction at the MRCI/a5Z level. What is remarkable, however, is that the same PEP is obtained at the single reference RCCSD(T)/a5Z level, which, disregarding the energy shift, is identical to the MRCI one, hence in defense of Scheme 1b. On the other hand, a detailed analysis of the Mulliken populations along the MRCI PEP suggests that the best way of representing the equilibrium electronic structure of the $\tilde{X}^3\Sigma^-$ state of CNN is by the vbL diagram of Scheme 5.

The numbers 0.70 and 0.20, and 0.60 indicate electron transfer through the π and σ systems, respectively. Notice also that the two triplet-coupled electrons are localized on the C and $N_{(b)}$ end atoms of the molecule not both on the C atom as indicated in Scheme 1b.

Incidentally, the $^3\Sigma^-$ PEP of CNN at the r(C−NN) distance of about 2.6 Å shows van der Waals interactions of 380 and 503 cm^{-1} at the MRCI and RCCSD(T)/a5Z levels, respectively.

Here, we must take up the $\tilde{X}^3\Sigma^-$ state of the CCO molecule. Table 3b lists our numerical findings at the MRCI+Q and RCCSD(T)/a5Z levels of theory. At the coupled-cluster level, we predict r_e(C−CO) = 1.3677 Å, r_e(CC−O) = 1.1598 Å, $D_e^\circ(D_0^\circ)$ = 53.3(50.8) kcal/mol, and μ_e = 1.52 D, exactly twice the corresponding μ_e of CNN. Our RCCSD(T) value of D_0° = 50.8 kcal/mol is in excellent agreement with the experimental value of the Neumark group D_0° = 51.7 ± 0.5

DOI: 10.1021/acs.jpca.9b09084
J. Phys. Chem. A 2019, 123, 10290−10302

Table 3. (a) Total Energies E (E_h), Bond Distances r_e (Å), Dissociation Energies D_e and D_0 (kcal/mol), and Harmonic Frequencies ω_e (cm^{-1})[a] of the Ground $\tilde{X}^3\Sigma_g^-$ State of the NCN Diradical[l]; (b) Total Energies E (E_h), Bond Distances r_e (Å), Dissociation Energies D_e and D_0 (kcal/mol), Harmonic Frequencies ω_e (cm^{-1}),[a] and Electric Dipole Moments μ_e (D) of the Ground $\tilde{X}^3\Sigma^-$ State of the CCO Diradical

(a) ground $\tilde{X}^3\Sigma_g^-$ state of the NCN diradical

method	$-E$	r_e(N−CN)	D_e[b]	D_0[b]	$\omega_1(\sigma_g^+)$, $\omega_2(\pi_u)$, $\omega_3(\sigma_u^+)$
MRCI	147.27256	1.2316	108.2	106.3	1219.4, 420.5, 1321.0
MRCI+Q	147.3014	1.232	108.9	107.0[c]	
RCCSD(T)	147.30223	1.2308	110.1	108.2[c]	
MRD-CI+Q[d]	147.245676	1.2404			1221, 417, 1329
expt.		1.230944(14)[e]		105.2 ± 0.92[f]	1197,[g] 437,[g] 1466.5[g]

(b) ground $\tilde{X}^3\Sigma^-$ state of the CCO diradical

method	$-E$	r_e(C−CO)	r_e(CC−O)	D_e[b]	D_0[b]	μ_e[h]	$\omega_1(\sigma^+)$, $\omega_2(\pi)$, $\omega_3(\sigma^+)$
MRCI	151.03615	1.3571	1.1596	49.4	46.9	1.58	
MRCI+Q	151.0672	1.364	1.163	52.1	49.6	1.47	
RCCSD(T)	151.07236	1.3677	1.1598	53.3	50.8	1.52	1077.3, 393.2, 2035.0
RCCSD(T)/TZ3P(2f)[i]	151.027818	1.3699	1.1627	52.93[j]	50.3[j]	1.47	1066, 455, 2003
expt.					51.7 ± 0.5[k]		1063,[g] 379.53,[g] 1970.86[g]

[a] $\omega_1(\sigma^+$; symmetric stretch), $\omega_2(\pi$; bend), $\omega_3(\sigma^+$; antisymmetric stretch). [b] Dissociation energy of NCN($\tilde{X}^3\Sigma_g^-$) with respect to C(^{3}P) + CN($X^2\Sigma^+$) and of CCO($\tilde{X}^3\Sigma^-$) with respect to C(^{3}P) + CO($X^1\Sigma^+$). [c] Zero point energy of NCN; ZPE = 1690.7 cm^{-1} at the MRCI level. [d] Ref 20. Basis set $[6s4p2d2f]_{N,C}$. MRD-CI is the Buenker−Peyerimoff multireference method. [e] Ref 42. [f] Ref 43. [g] Ref 26. [h] Dipole moment of CCO through the finite field approach. [i] Ref 31. TZ3P(2f) = $[5s3p3d2f]_{C,O}$. [j] Dissociation energies through cc-pVQZ//TZ3P(2f). [k] Ref 44. D_0 with respect to C(^{3}P) + CO($X^1\Sigma^+$). [l] Experimental and most recent theoretical results are also included for comparison.

Scheme 5. Electronic Structure of CNN($\tilde{X}^3\Sigma^-$) through its vbL Diagram

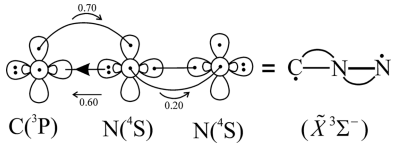

kcal/mol.[44] It is interesting to observe that the equilibrium bond distance r_e(CC−O) = 1.1598 Å is just 0.031 Å larger than that of the free CO($X^1\Sigma^+$),[30] an expected small bond lengthening indicating that the vbL diagram of Scheme 4 is a reasonable zero-order description of the $\tilde{X}^3\Sigma^-$ state of CCO. In contrast to the CNN case, we conclude that both triplet-coupled electrons are localized on the first carbon atom ($C_{(a)}$), that the in situ CO retains its "triple" bond character, and that the vbL diagrams of Schemes 4 (CCO) and 5 (CNN) depict vividly the bonding differences between the $\tilde{X}^3\Sigma^-$ states of CCO and CNN.

We turn now to the next triplet of CNN, $\tilde{A}^3\Pi$, about 23 850 cm^{-1} above the ground state.[14] The main equilibrium MRCI configuration function and the Mulliken atomic distributions are

$$|\tilde{A}^3\Pi\rangle \approx 0.92|(\text{core})^6 4\sigma^2 5\sigma^2 6\sigma^2 7\sigma^1 1\pi^4 2\pi^3\rangle$$

$$2s^{0.98}2p_z^{0.68}2p_x^{1.23}2p_y^{0.84}/_C 2s^{1.27}2p_z^{1.05}2p_x^{1.26}2p_y^{1.35}/_{N(a)} 2s^{1.92}2p_z^{1.10}2p_x^{0.91}2p_y^{1.41}/_{N(b)}$$

with net Mulliken charges $+0.27/_C$ $+0.07/_{N(a)}$ $-0.34/_{N(b)}$. The configuration above is the $B_1(x)$ component of the Π state and thus the asymmetry between the $2p_x$ and $2p_y$ atomic electron distributions. Taking into account the $B_2(y)$ component, the $2p_x$ and $2p_y$ distributions should read $2p_x^{1.04}2p_y^{1.04}/_C$ $2p_x^{1.30}2p_y^{1.30}/_{N(a)}$ $2p_x^{1.16}2p_y^{1.16}/_{N(b)}$.

According to Table 2, our "best" RCCSD(T)/a6Z equilibrium bond lengths r_e(C−NN) and r_e(CN−N) are 1.2212 and 1.1792 Å, respectively, about 0.02 Å shorter than the corresponding bond distances of the $\tilde{X}^3\Sigma^-$ state. With respect to C(^{3}P) + $N_2(X^1\Sigma_g^+)$, the RCCSD(T)/a6Z dissociation energy is $D_0°$(C−NN) = −39.0 kcal/mol, meaning that the $\tilde{A}^3\Pi$ state is unbound with respect to the ground state asymptotic products. Actually, according to the fully optimized MRCI PEP of Figure 1, an avoided interaction around r(C−NN) = 1.6 Å is responsible for trapping the molecule in the $\tilde{A}^3\Pi$ state. At the MRCI/a5Z level of theory and at r(C−NN) = 1.65 Å, a well depth ("barrier" from the left) of 60.7 kcal/mol is predicted. Depending on the vibrational state of the CNN species in the $\tilde{A}^3\Pi$ state, a penetration amplitude $\langle$C(^{3}P) + $N_2(X^1\Sigma_g^+)|$CNN($\tilde{A}^3\Pi$)$\rangle$ is possible that could give rise to a predissociation during the A ← X transition. In a photodissociation dynamics experiment of the CNN radical by Neumark and co-workers,[14] it is stated that "our results suggest that the $\tilde{A}^3\Pi$ state is subject to a barrier to dissociation approximately 1000 cm^{-1} above its vibrational ground state", corroborating, albeit qualitatively, our findings. With respect to C(^{3}P)+ $N_2(X^1\Sigma_g^+)$, the barrier is 96.9 kcal/mol.

The question from where this barrier comes from arises naturally. Figure 3 shows large state-averaged (B_1 and B_2 components) CASSCF/a5Z PEP calculations (71 860 CFs) of four $^3\Pi$ states, namely, $\tilde{A}^3\Pi$, $2^3\Pi$, $3^3\Pi$, and $4^3\Pi$, correlating to C(^{3}P) + $N_2(X^1\Sigma_g^+$, $A^3\Sigma_u^+$, $B^3\Pi_g$, and $w^3\Delta_u$), respectively. Observe first that at large r(C−NN) distances the T_e experimental energy differences $N_2(A^3\Sigma_u^+$, $B^3\Pi_g$, $w^3\Delta_u)$ − $N_2(X^1\Sigma_g^+)$ = 50 203.6, 59 619.3, and 59 908 cm^{-1} [30] are compared favorably with the CASSCF numbers 46 217, 58 777, and 59 469 cm^{-1}, respectively. Relatively small discrepancies between experiment and theory are due mainly to the absence of dynamical correlation differential effects.

The CASSCF potential energy profiles look "messy", but one thing is clear: the barrier of the $\tilde{A}^3\Pi$ state is the result of consecutive "avoided crossings" among the $3^3\Pi$, $2^3\Pi$, and $\tilde{A}^3\Pi$ states, which means that the structural electronic features of the $3^3\Pi$ and perhaps those of $4^3\Pi$ states are conveyed to the equilibrium structure of $\tilde{A}^3\Pi$.

A final word should be added as to the electrical dipole moment of the $\tilde{A}^3\Pi$ state. Both MRCI+Q and coupled-cluster

DOI: 10.1021/acs.jpca.9b09084
J. Phys. Chem. A 2019, 123, 10290−10302

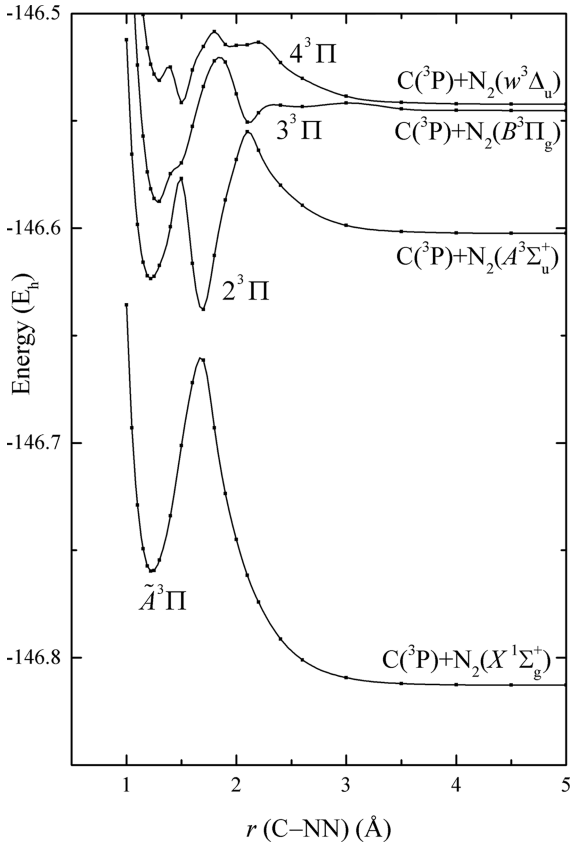

Figure 3. Potential energy profiles of four $^3\Pi$ states of CNN correlating to C(^{3}P) + N$_2$($X^1\Sigma_g^+$, $A^3\Sigma_u^+$, $B^3\Pi_g$, $w^3\Delta_u$) at the CASSCF/a5Z level; see the text.

calculations predict its magnitude to be μ_e = 2.06−2.07 D, in complete agreement with ref 21, but with opposite sign with respect to the μ_e (=0.76 D) of the $\tilde{X}^3\Sigma^-$ state (Table 2), while the ratio $\mu_e(\tilde{A}^3\Pi)/\mu_e(\tilde{X}^3\Sigma^-) \approx 3$ points to a much polar $\tilde{A}^3\Pi$ state. Our finite field calculations leave no doubt that the polarity of the $\tilde{A}^3\Pi$ state is $^{(+)}$C−NN$^{(-)}$ in agreement with the Mulliken population analysis.

4.1.2. $\tilde{a}^1\Delta$, $\tilde{b}^1\Sigma^+$, and $\tilde{c}^1\Pi$. All singlets correlate adiabatically to C(^{1}D) + N$_2$($X^1\Sigma_g^+$). The leading MRCI equilibrium configuration of the $\tilde{a}^1\Delta$ state and its atomic Mulliken distributions are

$$|\tilde{a}^1\Delta\rangle \approx 0.66|(\text{core})^6 4\sigma^2 5\sigma^2 6\sigma^2 7\sigma^2 1\pi^4(2\pi_x^2 - 2\pi_y^2)\rangle$$

$$2s^{1.67}2p_z^{0.93}2p_x^{0.65}2p_y^{0.65}/_{C}2s^{1.30}2p_z^{1.06}2p_x^{1.27}2p_y^{1.27}/_{N(a)}2s^{1.92}2p_z^{1.13}2p_x^{1.08}2p_y^{1.08}/_{N(b)}$$

The correct description of the $\tilde{a}^1\Delta$ symmetry, however, requires also the intermingling of the "open" singlet configuration $...7\sigma^2 1\pi^4(2\pi_x^{\uparrow}2\pi_y^{\downarrow} - 2\pi_x^{\downarrow}2\pi_y^{\uparrow})$ (see below). Now, in the $\tilde{b}^1\Sigma^+$ state, the "−" sign becomes "+" and of course "the open singlet" component is missing. The net Mulliken charges are identical for both the $\tilde{a}^1\Delta$ and $\tilde{b}^1\Sigma^+$ states, i.e., $+0.1/_{C}$ $+0.1/_{N(a)}$ $-0.2/_{N(b)}$. The dipole moment diminishes by about 0.2 D as we move from the $\tilde{X}^3\Sigma^-$ state to $\tilde{a}^1\Delta$ and $\tilde{b}^1\Sigma^+$. The MRCI(+Q) geometries are in complete agreement with Ornellas and co-workers,[24] while adiabatic dissociation energies D_e (D_0), fundamental harmonic frequencies (ω_1, ω_2, and ω_3), and dipole moments have been computed for the first time; see Table 2. Experimental energy gaps (T) $\tilde{a}^1\Delta - \tilde{X}^3\Sigma^-$ and $\tilde{b}^1\Sigma^+ - \tilde{X}^3\Sigma^-$ recorded for the first time by Clifford at al.[13] are 6830 ± 120 and 10 690 ± 120 cm^{-1}, respectively, are in harmony with the present MRCI+Q T_0 numbers; see Table 2. The $\omega_3(\sigma^+)$ experimental[13] asymmetric stretching of 1600 ± 120 cm^{-1} is in relative agreement with our (harmonic) 1907 cm^{-1} value. Finally, we would like to make some comments on the fully optimized PEPs of the $\tilde{a}^1\Delta$ and $\tilde{b}^1\Sigma^+$ states of Figure 1.

As was already mentioned, the three singlets correlate adiabatically to the first excited state of the carbon atom ^{1}D ($2s^22p^2$), experimentally 29.14 kcal/mol[45] above the ground ^{3}P state, and N$_2$($X^1\Sigma_g^+$). At "infinity" (∼10 Å), the MRCI ^{1}D−^{3}P gap is calculated to be 30.1 kcal/mol. The axial ($C_{\infty v}$) projection of the ^{1}D symmetry state gives rise to Δ, Π, and Σ symmetries. Therefore, the linear approach of the $X^1\Sigma_g^+$ state of N$_2$ to the ^{1}D state of carbon gives rise to the singlets $^1\Delta$, $^1\Pi$, and $^1\Sigma^+$ with |Λ| = 2, 1, and 0, respectively. The formation of the $\tilde{a}^1\Delta$ and $\tilde{b}^1\Sigma^+$ states from C(^{1}D; M_L = ±2, 0) + N$_2$($X^1\Sigma_g^+$) is shown in the vbL diagrams of Scheme 6.

Scheme 6. VbL Diagrams Referring to the Formation of the $\tilde{a}^1\Delta$ and $\tilde{b}^1\Sigma^+$ States of CNN

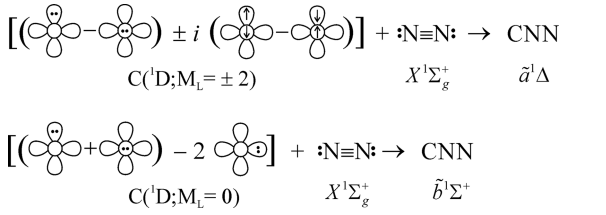

Notice the imaginary component of the "open singlet" of the C(^{1}D; M_L = ±2) vbL diagram of the $\tilde{a}^1\Delta$ state. Observe the sizeable energy barrier of 18.0 kcal/mol of the $\tilde{b}^1\Sigma^+$ state around r(C−NN) = 2.0 Å to be contrasted with the barrierless PEP of the $\tilde{a}^1\Delta$ state; Figure 1. Taking into account the $\tilde{a}^1\Delta$ vbL diagram of Scheme 6 and that the bond lengths r_e(C−NN) and r_e(CN−N) do not differ substantially from those of the $\tilde{X}^3\Sigma^-$ state, we dare suggest that the electronic equilibrium structure of $\tilde{a}^1\Delta$ could be represented by the diagram of Scheme 5 but with the two end-electrons coupled into a singlet.

The situation of the $\tilde{b}^1\Sigma^+$ singlet is different. The approach of N$_2$($X^1\Sigma_g^+$) to the carbon ^{1}D(M_L = 0) state from "infinity" up to r(C−NN) of about 2.0 Å is repulsive, while the r(CN−N) distance remains essentially constant and equal to 1.10 Å, the bond length of the free N$_2$.[30] Having past the r(C−NN) ≈ 2.0 Å point, the potential energy function becomes attractive with the in situ r(CN−N) distance increasing gradually to the final equilibrium value of 1.18 Å at r(C−NN) = 1.27 Å; see Figure 1 and Table 2. The cause of the barrier is rather due to the repulsive interaction of the σ^2 (∼$2s^2$) electron distribution of N$_2$ and the $2p_z^2$ part of the C(^{1}D;M_L = 0) along the $\tilde{b}^1\Sigma^+$ profile; see Scheme 6. Pushing further the N$_2$ moiety, the interaction becomes attractive, forming a "dative" bond.

The equilibrium bond lengthening of CN−N by 0.08 Å relative to the bond distance of free N$_2$ could be attributed to, perhaps, the nonbonding interaction of the $\pi_{x,y}$ systems of C and N$_2$.

The third of the singlets, $\tilde{c}^1\Pi$, correlating adiabatically to C(^{1}D; M_L = ±1) + N$_2$($X^1\Sigma_g^+$), lies 26.5 kcal/mol above the $\tilde{A}^3\Pi$ state at the MRCI/a5Z level. We are not aware of any experimental information on the $\tilde{c}^1\Pi$ state. Theoretically, the only result known is the vertical excitation energy $T_v(\tilde{c}^1\Pi \leftarrow$

DOI: 10.1021/acs.jpca.9b09084
J. Phys. Chem. A 2019, 123, 10290−10302

$\tilde{X}^3\Sigma^-$) = 34 085 cm^{-1} at the MRCI+Q/CBS$_{T\text{-}5}$ level of theory.[24]

The main MRCI equilibrium configuration function and corresponding atomic Mulliken populations are

$$|\tilde{c}^1\Pi\rangle \approx 0.88|(\text{core})^6 4\sigma^2 5\sigma^2 6\sigma^2 7\sigma^1 1\pi^4 2\pi^3\rangle$$

$$2s^{0.99}2p_z^{0.70}2p_x^{1.17}2p_y^{0.75}/_C\ 2s^{1.29}2p_z^{1.06}2p_x^{1.36}2p_y^{1.28}/_{N(a)}2s^{1.95}2p_z^{1.01}2p_x^{1.47}\ 2p_y^{0.95}/_{N(b)}$$

with Mulliken charges $+0.39/_C$ $-0.01/_{N(a)}$ $-0.38/_{N(b)}$. Our MRCI(+Q) results given in Table 2 read r_e(C−NN) = 1.1823(1.185) Å, r_e(CN−N) = 1.2545(1.255) Å, and D_e = −32.6(−33.8) kcal/mol with respect to C(^{1}D) + N$_2$($X^1\Sigma_g^+$); for technical reasons, fundamental vibrational frequencies have been obtained at the MRCI/aug-cc-pVTZ level. The potential energy function shown in Figure 1 is very similar to that of the $\tilde{A}^3\Pi$ state. Indeed, as the N$_2$ molecule approaches the C(^{1}D; $M_L = \pm 1$) atom from infinity in a linear fashion, its PEP is strongly repulsive up to r(C−NN) = 1.60 Å where it suffers a "repulsive interaction" possibly with a $^1\Pi$ state correlating to C(^{1}D) + N$_2$($a'^1\Sigma_u^-$), experimentally 8.45 eV above the C(^{1}D) + N$_2$($X^1\Sigma_g^+$) asymptote.[30] It is interesting to observe that the experimental bond length of the $a'^1\Sigma_u^-$ state of free N$_2$ is equal to 1.2755 Å,[30] a mere 0.021 Å longer than the MRCI r_e(CN−N) value of the $\tilde{c}^1\Pi$ state. Having past the r(C−NN) = 1.60 Å point, the "repulsive interaction" with the higher-lying incoming $^1\Pi$ state creates a potential well of 70.3 kcal/mol, trapping the CNN molecule in the $\tilde{c}^1\Pi$ state. The barrier with respect to the asymptote C(^{1}D) + N$_2$($X^1\Sigma_g^+$) is 103.4 kcal/mol. These two numbers should be compared with those of the $\tilde{A}^3\Pi$ state, 60.7 and 96.9 kcal/mol, respectively (vide supra). The MRCI excitation energy $T_e(\tilde{c}^1\Pi - \tilde{X}^3\Sigma^-)$ is 32 737 cm^{-1} in logical accord with the corresponding vertical value of the Ornellas group,[24] T_v = 34 085 cm^{-1}.

Before leaving the $\tilde{c}^1\Pi$ state, a comment is in order for the (finite field) dipole moment, its MRCI value being −2.80 D (Table 2). The polarity of the molecule is $^{(+)}$C−N$_2^{(-)}$ in agreement with the Mulliken charges, suggesting a strongly polar state.

4.2. NCN. Experimental results on seven states of the centrosymmetrical isomer of CN$_2$, NCN($\tilde{X}^3\Sigma_g^-$, $\tilde{a}^1\Delta_g$, $\tilde{b}^1\Sigma_g^+$, $\tilde{A}^3\Pi_u$, $\tilde{B}^3\Sigma_g^-$, $\tilde{c}^1\Pi_u$, $\tilde{d}^1\Delta_u$), mainly vibrational frequencies ($\omega_1(\sigma_g^+)$, $\omega_2(\pi_u)$, $\omega_3(\sigma_u^+)$) and energy separations (T_0) among the states above, can be found in the Jacox compilation.[26] Here, we are only interested in the $\tilde{X}^3\Sigma_g^-$ state of NCN and its relation to the $\tilde{X}^3\Sigma^-$ state of CNN. The X-state symmetry of NCN was predicted theoretically at the SCF/DZ +P (Slater basis set) level by Thomson in 1973,[6] whereas the best ab initio calculations so far around the equilibrium at the MRD-CI/[6s4p2d2f]$_{N,C}$ level are those of Pd and Chandra in 2001;[20] see also Table 3.

The leading equilibrium MRCI configuration function of the $\tilde{X}^3\Sigma_g^-$ state of NCN and its atomic Mulliken populations are

$$|\tilde{X}^3\Sigma_g^-\rangle \approx 0.895|(\text{core})^6 3\sigma_g^2 4\sigma_g^2 2\sigma_u^2 3\sigma_u^2 1\pi_u^4 1\pi_g^2\rangle$$

$$2s^{0.88}2p_z^{0.90}2p_x^{0.98}2p_y^{0.98}/_C 2s^{1.73}2p_z^{1.38}2p_x^{1.01}2p_y^{1.01}/_N$$

where $(\text{core})^6 = 1\sigma_g^2 2\sigma_g^2 1\sigma_u^2$ and $-0.13/_N$ $+0.26/_C$ $-0.13/_N$ are the net Mulliken charges. The vbL diagram of Scheme 3 shows succinctly the electronic structure of the ground state with the triplet-coupled electrons localized on the nitrogen atoms. It is important to be realized that the in situ C atom in NCN is in the (third) excited ^{5}S ($2s^1 2p^3$) state 96.4 kcal/mol above its ^{3}P ground state,[45] as opposed to the C atom of CNN($\tilde{X}^3\Sigma^-$) with the in situ C atom in the ground ^{3}P state (vide supra). Apart from the "nonbonding" triplet-coupled electrons, the bonding in NCN is "identical" to that of the O═C═O ($\tilde{X}^1\Sigma_g^+$) molecule; recall that the in situ C atom in CO$_2$ is in the ^{5}S state as well.[46]

The relatively high electron affinities (EA) of NCN($\tilde{X}^3\Sigma_g^-$) and HNCN($\tilde{X}^2A''$) according to the photoelectron spectroscopic results of Clifford et al.,[47] EA = 2.484 ± 0.006 and 2.622 ± 0.005 eV, respectively, are in support of the electronic structure of NCN shown in the diagram of Scheme 3.

Table 3 collects our numerical results on the $\tilde{X}^3\Sigma_g^-$ state of NCN, and Figure 4 shows the CASSCF(142 000 CFs)/a5Z

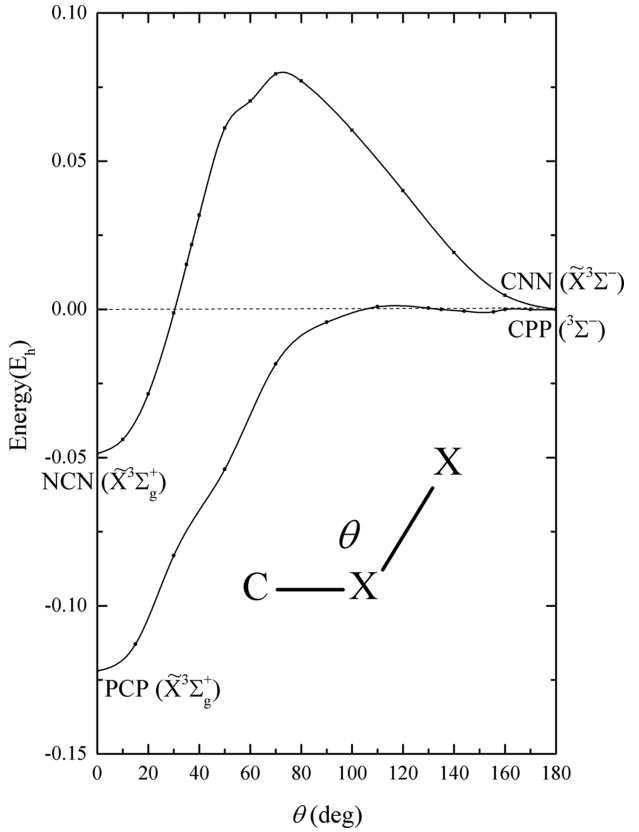

Figure 4. Fully optimized potential energy profiles of the isomerization process CXX to XCX, where X = N and P at the CASSCF/a5Z level; see the text.

PEP of the isomerization process CNN($\tilde{X}^3\Sigma^-$) → NCN-($\tilde{X}^3\Sigma_g^-$), as the angle θ ($\angle$CN$_{(a)}$N$_{(b)}$) sweeps out the range 180.0 (CNN) to 0.0° (NCN) on the triplet C_s surface. As the N$_{(b)}$ atom swings from θ = 180 to 73°, the barrier is 50 kcal/mol, whereas from 0.0 to 73°, the well depth is 81 kcal/mol. The stability of NCN($\tilde{X}^3\Sigma_g^-$) over CNN($\tilde{X}^3\Sigma^-$) by about 30−31 kcal/mol is confirmed at all levels of highly correlated methods; see Tables 2 and 3. Therefore, between the two isomers of CN$_2$, CNN and NCN, the latter is the global minimum. The 50 kcal/mol energy barrier is the result of the C atom transformation from "divalent" (^{3}P) to "tetravalent" (^{5}S) and to the concomitant bond breaking and forming through this path.

With the exception of the antisymmetric stretch $\omega_3(\sigma_u^+)$ calculated 146 cm^{-1} lower than the experimental value, our results are in excellent agreement with the experiment (Table

DOI: 10.1021/acs.jpca.9b09084
J. Phys. Chem. A 2019, 123, 10290−10302

3). The MRCI (MRCI+Q) [RCCSD(T)] r_e(N−CN) is 1.2316 (1.232) [1.2308] Å consistent within 0.001 Å in all methods and in perfect agreement with the experimental value of Beaton et al. of 1.230944(14) Å.[42] The PEP CN($X^2\Sigma^+$)+N(^{4}S) is given in Figure 5. According to Table 3, the NC−N

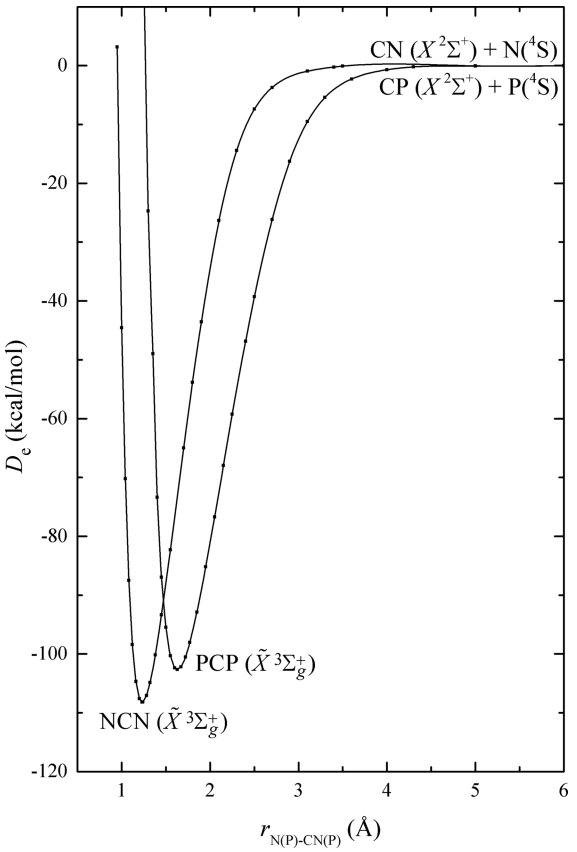

Figure 5. Fully optimized potential energy profiles of the dissociation processes XCX($\tilde{X}^3\Sigma_g^-$) to CX($X\,^2\Sigma^+$) + X(^{4}S), where X = N and P at the MRCI/a5Z level.

dissociation energy $D_e°/D_0°$ at the MRCI (MRCI+Q) [RCCSD(T)] methodologies is 108.2 (108.9) [110.1]/106.3 (107.0) [108.2] kcal/mol, as compared to the experimental value $D_0°$ = 105.2 ± 0.92 kcal/mol of Neumark and co-workers.[43] Finally, an atomization energy (NCN → C(^{3}P) + 2N(^{4}S)) D_0^{at} = 282.9 kcal/mol is obtained at the RCCSD(T)/a5Z level (Table 4).

4.3. c-CN_2. The cyclic isomer c-CN_2 (cyclic "carbene") has a singlet ground state and a geometry of C_{2v} symmetry.[18] The purpose of its study in the present report at the RCCSD(T)/a5Z level is, mainly, for reasons of completeness and uniformity. The best ab initio calculations so far on the $\tilde{X}^1A_1$ state of c-CN_2 are those of Martin et al.[18] at the CASSCF/pVDZ and CCSD(T)/TZ2P levels. The singlet c-CN_2 carbene has been observed recently in solution[48] and in the gas phase,[49] thus confirming the previous[18] and present ab initio calculations.

It is useful to draw a vbL diagram of the $^1A_1$ state of c-CN_2, predicting, at least in principle, its stability on the singlet potential surface; Scheme 7.

Scheme 7. vbL Diagram of c-CN_2($\tilde{X}^1A_1$)

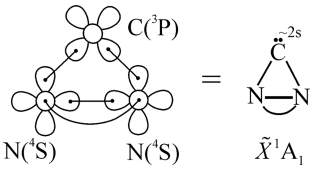

Our results at the RCCSD(T)/a5Z (valence) level are given in Table 5 along with the results of Martin et al.[18] for easy comparison. It is interesting that the $\tilde{X}^3\Sigma^-$ and $\tilde{X}^1A_1$ states of CNN and c-CN_2, respectively, are practically isoenergetic. In fact, the latter is more stable than the former by 2.5 mE_h (=1.7 kcal/mol) at the RCCSD(T)/a5Z level (Tables 2 and 5), but remember that we are referring to potential surfaces of different spin multiplicities. It should also be mentioned that the polarity of c-CN_2 is clearly $^{(-)}$C−N$_2^{(+)}$ according to the dipole moment finite field calculations.

A final word as to the bonding of c-CN_2 is needed. This cyclic species is isoelectronic to the cyclopropene carbene C(CH)$_2$. The C(CH)$_2$ molecule was examined through ab initio calculations, namely, QCISD(T)//MP2/6-31G(d′) and MP4(SDQ)/CBS4, MP2/CBS3//MP2/6-31G(d′) methods by Jursic in 1999.[50] The conventional geometrical structure of the singlet (C_{2v}; $\tilde{X}^1A_1$) cyclopropene carbene according to Jursic is shown in Scheme 8.

Note that the in situ unique C atom is in the ^{3}P ground state, the isoelectronic to N(^{4}S) in situ CH moieties in the $a^4\Sigma^-$ state 17.5 kcal/mol above the X $^2\Pi$ state,[51] while the in

Table 4. Total Energies E (E_h), Bond Distances r_e (Å), Dissociation Energies D_e and D_0 (kcal/mol), Harmonic Frequencies ω_e (cm^{-1}),[a] and Electric Dipole Moments μ_e (D) of the Ground States of the CPP($\tilde{X}^3\Pi$) and PCP($\tilde{X}^3\Sigma_g^-$) Diradicals at the MRCI/a5Z and RCCSD(T)/a5Z Levels

method	−E	r_e(C−P)	r_e(P−P)	D_e[b]	D_0[b]	μ_e[c]	$\omega_1(\sigma^+)$, $\omega_2(\pi)$, $\omega_3(\sigma^+)$
			CPP($\tilde{X}^3\Pi$)				
MRCI	719.60044	1.5711	1.9906	7.0	5.0	0.21	511,[d] 229/254,[d] 1179[d]
MRCI+Q	719.6394	1.574	1.991	8.2	6.2	0.32	
RCCSD(T)	719.63971	1.5718	1.9771	9.3	7.3	0.305	532,[d] 248,[d] 1120[d]
			PCP($\tilde{X}^3\Sigma_g^-$)				
MRCI	719.77169	1.6289		102.7	101.6	0.0	582,[d,e] 264,[d,e] 909[d,e]
MRCI+Q	719.8087	1.630		103.8	102.7	0.0	
RCCSD(T)	719.81204	1.6276		105.1	104.0	0.0	

[a] $\omega_1(\sigma^+$; symmetric stretch), $\omega_2(\pi$; bend), $\omega_3(\sigma^+$; antisymmetric stretch). [b] Dissociation energy of CPP($\tilde{X}^3\Pi$) with respect to C(^{3}P) + P$_2$($X^1\Sigma^+$) and of PCP($\tilde{X}^3\Sigma_g^-$) with respect to CP($X^2\Sigma^+$) + P(^{4}S). [c] Dipole moment of CPP through the finite field approach. [d] ZPE of CPP, 1087 (MRCI), 1074 (RCCSD(T)) cm^{-1}; ZPE of PCP, 1010 cm^{-1}. [e] CASSCF values.

DOI: 10.1021/acs.jpca.9b09084
J. Phys. Chem. A 2019, 123, 10290−10302

Table 5. Total Energies E (E_h), Geometry r_e (Å) and θ (∠NCN) (degrees), Bond Dissociation Energies D_e and D_0 (kcal/mol), Harmonic Frequencies ω_1, ω_2, ω_3 (cm^{-1}), and Electric Dipole Moments μ_e (D) of the Ground $\tilde{X}^1A_1$ State of the c-CN2 Molecule at the RCCSD(T)/a5Z Level[d]

method	$-E$	r_e(C−N)	r_e(N−N)	θ	D_e[a]	D_0[a]	μ_e[b]	$\omega_1(a_1)$, $\omega_2(b_2)$, $\omega_3(a_1)$
RCCSD(T)	147.25662	1.3907	1.2844	55.0	33.2	31.3	0.55	1117, 1007, 1560
CCSD(T)[c]	147.21607	1.3979	1.2921	55.05				1084.3, 973.5, 1521.9

[a]Dissociation energy with respect to $C(^3P) + N_2(X^1\Sigma_g^+)$. [b]Electric dipole moment through the finite field approach. [c]Ref 18; TZ2P basis set. [d]Theoretical results are also included from the literature.

Scheme 8. Conventional Chemical Formula of $C(CH)_2(^1A_1)$

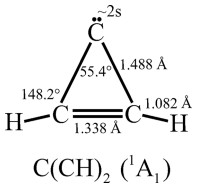

$C(CH)_2$ ($^1A_1$)

situ C-atoms (of the CH groups) trace their ancestry to their third ^5S excited state. The comparison of Schemes 7 and 8 and the geometries of c-CN_2 (Table 5) and $C(CH)_2$ (Scheme 8) shows that the bonding of both species is of similar nature.

4.4. CPP and PCP. *4.4.1. CPP.* As was already mentioned for the phosphorous isovalent analogue of CN_2, carbon diphosphide, CP_2, we are aware of only two experimental studies published some 50 years ago.[28,29] Independently on their conclusions as to the stability of the two isomers (see the "Introduction"), the atomization energy given by both groups is quite realistic (see below).

Concerning now the CPP isomer, and by analogy to CNN (see also Section 2), we examined by the MRCI/a5Z approach the symmetries $^3\Sigma^-$, $^1\Delta$, $^1\Sigma^+$, and $^3\Pi$. The potential energy profiles of $^3\Sigma^-$ [$C(^3P) + P_2(X^1\Sigma_g^+)$], $^1\Delta$, $^1\Sigma^+$ [$C(^1D) + P_2(X^1\Sigma_g^+)$], and $^3\Pi$ [$C(^3P) + P_2(X^1\Sigma_g^+)$] are displayed in Figure 6; notice that the first three PEPs are shown in dashed lines but the fourth one ($^3\Pi$) in solid line (but see below). Disregarding the energy shifts (P_2 instead of N_2), the similar morphologies of the CPP and CNN PEPs are indeed striking in every respect; compare Figures 1 and 6. There is a catch however: the three CPP "states" $^3\Sigma^-$ (correlating to the ground-state fragments), $^1\Delta$, and $^1\Sigma^+$ have one imaginary fundamental frequency, specifically the bending one, $\omega_2(\pi)$, referring to saddle points of order one. This in turn means that the lowest stationary state of the CPP molecule with all three fundamental frequencies real (Table 1) is of $\tilde{X}^3\Pi$ symmetry with its PEP similar to the $\tilde{A}^3\Pi$ PEP of CNN, but with interesting numerical differences. Recall that the well depths of $\tilde{A}^3\Pi$ (CNN) are 60.7 kcal/mol and 96.9 kcal/mol from the right and up to 1.65 Å, hence unbound with respect to the asymptotic products $C(^3P) + N_2(X^1\Sigma_g^+)$. On the contrary the corresponding well depth of CPP is 40.0 kcal/mol (onset of the "repulsive interaction" at 2.0 Å) and with $D_e°(D_0°)$ = 7.0(5.0) kcal/mol at the MRCI/a5Z level with respect to the asymptotic products $C(^3P) + P_2(X^1\Sigma_g^+)$. As our "best" estimate of the C−P_2 dissociation energy $D_e°(D_0°)$, we suggest the values 9.3(7.3) kcal/mol; see Table 4.

Now the leading equilibrium MRCI configuration and atomic Mulliken distribution of the $\tilde{X}^3\Pi$ (Π_x; B_1 component) state of $CP_{(a)}P_{(b)}$ are

$$|\tilde{X}^3\Pi\rangle \approx 0.86|(\text{core})^{22}8\sigma^2 9\sigma^2 10\sigma^2 11\sigma^1 3\pi^4 4\pi^3\rangle$$
$$2s^{1.36}2p_z^{0.78}2p_x^{0.92}2p_y^{1.18}/_C 3s^{1.30}3p_z^{0.79}3p_x^{1.16}3p_y^{1.26}/_{P(a)} 3s^{1.82}3p_z^{0.94}3p_x^{0.95}3p_y^{1.54}/_{P(b)}$$

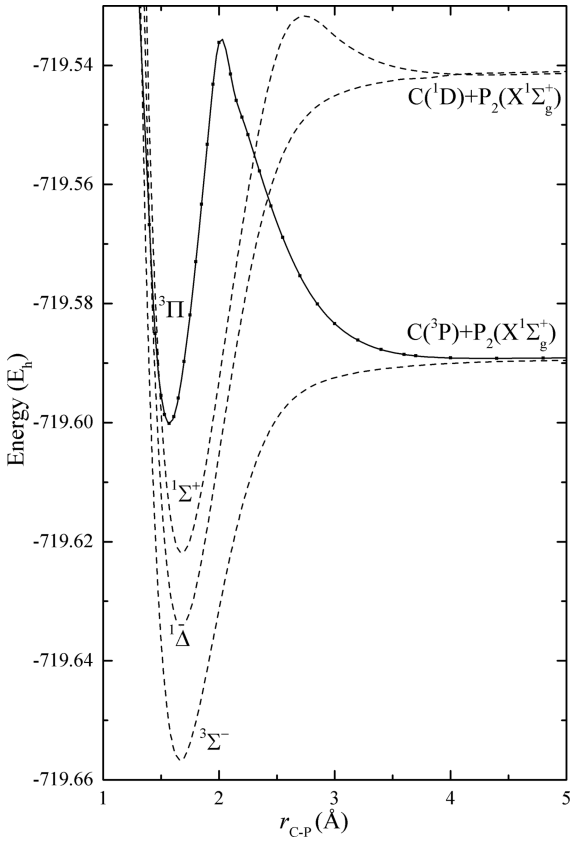

Figure 6. Fully optimized potential energy profiles for the collinear approaches $C(^3P) + P_2(X^1\Sigma_g^+)$ and $C(^1D) + P_2(X^1\Sigma_g^+)$ at the MRCI/a5Z level of theory; see the text concerning dashed curves.

where $(\text{core})^{22} = 1\sigma^2 2\sigma^2 3\sigma^2 4\sigma^2 5\sigma^2 6\sigma^2 7\sigma^2 1\pi^4 2\pi^4$, with net Mulliken charges $+0.24/_C$ $+0.49/_{P(a)}$ $-0.25/_{P(b)}$. In agreement with the net Mulliken charges, a small dipole moment is expected, and this is what was found; μ_e = 0.31−0.32 D at the MRCI+Q or RCCSD(T) level of theory, about 7 times smaller and of opposite polarity to that of the $\tilde{A}^3\Pi$ state of CNN. Finally, the CP−P bond length, r_e = 1.9771 Å, is larger by 0.08 Å relative to the bond length of free $P_2(X^1\Sigma_g^+)$, r_e = 1.8934 Å,[30] equal to the CN−N($\tilde{A}^3\Pi$) bond lengthening relative to free $N_2(X^1\Sigma_g^+)$ at the same level of theory; see Tables 2 and 4.

4.4.2. PCP. According to our calculations, the symmetry of the ground state of the centrosymmetric isomer of CP_2, PCP, is $^3\Sigma_g^-$. Its electronic structure is represented succinctly by the vbL diagram of Scheme 3 with the P(^4S) atom replacing N(^4S). As in NCN($\tilde{X}^3\Sigma_g^-$), the in situ C atom is in the ^5S state and the two nonbonding electrons coupled into a triplet are localized on the two P atoms. Within 2 mE_h at all levels of theory of the present study, the $\tilde{X}^3\Sigma_g^-$ state of PCP is 107 kcal/mol lower than the $\tilde{X}^3\Pi$ state of CPP (Table 4). Mutatis-mutandis NCN is stabler than CNN, the corresponding energy

DOI: 10.1021/acs.jpca.9b09084
J. Phys. Chem. A 2019, 123, 10290−10302

difference $E(NCN; \tilde{X}^3\Sigma_g^-) - E(CNN; \tilde{A}^3\Pi)$ being −98 kcal/mol (Tables 2 and 3).

Figure 4 shows at the CASSCF/a5Z level the completely optimized energy profile of the isomerization procedure $CPP(^3\Sigma^-)$ to $PCP(\tilde{X}^3\Sigma_g^-)$ as a function of the angle θ (∠CXX), X = N or P. The comparison with $CNN(\tilde{X}^3\Sigma^-)$ to $NCN(\tilde{X}^3\Sigma_g^-)$ isomerization is quite interesting. As the $P_{(b)}$ atom swings from $\theta = 180°$ ($CP_{(a)}P_{(b)}$; $^3\Sigma^-$) to about 100°, the energy remains almost constant; a negligible energy dip of less than 1 mE_h around 155° is insignificant. From $\theta \approx 100$ to 0.0° (PCP; $\tilde{X}^3\Sigma_g^-$), the energy plummets barrierlessly and more or less linearly to the ground state of PCP, 107 mE_h (=67 kcal/mol) lower than the unstable (saddle point) $CPP(^3\Sigma^-)$; see Figure 4.

Figure 5 displays the MRCI dissociation profile D_e of $PCP(\tilde{X}^3\Sigma_g^-)$ with respect to $P(^4S) + CP(X^2\Sigma^+)$. Notice that the morphologies of the P−CP and N−CN PEPs are in essence identical, the MRCI/a5Z dissociation energies $D_e°(D_0°)$ being 102.7(101.6) and 108.2(106.3) kcal/mol, respectively.

Within reason the Mulliken population analysis of the fourteen valence electrons of $PCP(\tilde{X}^3\Sigma_g^-)$ is pretty close to that of $NCN(\tilde{X}^3\Sigma_g^-)$, while the net Mulliken charges are $-0.09/_P$ $+0.18/_C$ $-0.09/_P$ as compared to $-0.13/_N$ $+0.26/_C$ $-0.13/_N$ of NCN (vide supra).

After the previous exposition, the electronic structure similarity of the bonding between the X-states of PCP and NCN is rather obvious.

A final word is still needed. At the RCCSD(T)/a5Z level, the atomization energy of $PCP(\tilde{X}^3\Sigma_g^-) \rightarrow 2P(^4S) + C(^3P)$ is $D_0°$ (at) = $D_e°$ (at) − ZPE = 228.6 − 2.9 = 225.7 kcal/mol. The $D_0°$ (at) value combined with the experimental $\Delta_f H°$ values of P and C, 75.62 and 171.29 kcal/mol, respectively,[52] gives $\Delta_f H_0°$ (PCP) = 171.29 + 2 × 75.62−225.7 = 96.82 kcal/mol. Now, according to Smoes et al.,[28] the $D_0°$ (at) values of CPP and PCP are 230.2 ± 3.6 and 234.2 ± 3.6 kcal/mol, respectively, both numbers in good agreement with the theoretical $D_0°$ (at) = 225.7 kcal/mol given above. The authors suggest, however, that "it is likely that the molecule CP_2 observed is a mixture of both isomers".[28] One year later, Kordis and Gingerich, using essentially the same experimental thermochemical approach, reported $D_0°$ (at) = 231.9 ± 4.6 kcal/mol and $\Delta_f H_0°$ = 96.7 ± 2.5 kcal/mol.[29] It is important to say though that these authors favor, albeit mildly, the CPP isomer over the PCP one. Clearly, their $D_0°$ (at) is in accord with that of ref 28 and the present RCCSD(T) value. Observe that the experimental $\Delta_f H_0°$[29] is in perfect agreement with the RCCSD(T) value, $\Delta_f H_0°$ = 96.82 kcal/mol. The complete agreement between the experimental and theoretical $\Delta_f H°$ and the previous discussion on CPP and PCP show that the measurements of both experimental groups (refs 28 and 29) concern the centrosymmetric PCP isomer and clearly at the $\tilde{X}^3\Sigma_g^-$ state.

A theoretical work on $\Delta_f H°$ and the ionization energies of CP, PCP, and PCCP was published in 2000 by Fleming et al.[53] For the ground state of PCP, $\tilde{X}^3\Sigma_g^-$, at the RCCSD(T)/cc-pV5Z//UQCISD/6-311G(2d) level, they report $\Delta_f H_0°$ = 96 ± 2 kcal/mol quite in harmony with the present RCCSD(T)/a5Z result.

4.5. c-CP_2. We would like now to examine briefly the singlet cyclic isomer of CP, c-CP_2, a cyclic phosphorous "carbene". We are not aware of any previous work on c-CP_2 either experimental or theoretical.

By analogy to c-CN_2, we surmise a stable species (real fundamental vibrational frequencies), with a bonding structure represented by the vbL diagram of Scheme 7 ("P" instead of "N"). Our RCCSD(T)/a5Z (valence) calculations support the above conjectures.

The total equilibrium energy E; C_{2v} geometry r_e(C−P), r_e(P−P), and θ (∠PCP); dissociation energy D_e (and D_0) with respect to $C(^3P) + P_2(X^1\Sigma_g^+)$; harmonic vibrational frequencies (ω_1, ω_2, and ω_3); and the finite field dipole moment μ_e of the $^1A_1$ state of c-CP_2 are as follows: E = −719.78540 E_h, r_e(C−P) = 1.7860 and r_e(P−P) = 2.0454 Å, θ (∠PCP) = 69.9°, $D_e(D_0)$ = 45.2(43.2) kcal/mol, $\omega_1(a_1)$ = 601, $\omega_2(b_2)$ = 658, $\omega_3(a_1)$ = 872 cm^{-1}, and μ_e = 2.17 D.

The calculations of the finite field dipole moment show, with no doubt, that the polarity of the molecule is $^{(-)}C-P_2{}^{(+)}$, the same as that of c-CN_2 (vide supra).

5. CONCLUSIONS

Through variational multireference (MRCI) and coupled-cluster (RCCSD(T)) techniques and large cc basis sets (augmented quintuple and sextuple ζ), we studied the rather quixotic isovalent molecular systems CN_2 (CNN, NCN, c-CN_2) and CP_2 (CPP, PCP, c-CP_2), the latter, in essence, for the first time. The ground state of $CCO(\tilde{X}^3\Sigma^-)$, isoelectronic to CNN, was also examined for comparative reasons. Although these species cannot be considered as "chemically" very interesting, their bonding is intriguing and motivated the present work.

Specifically, for CNN, we have studied the states $\tilde{X}^3\Sigma^-$, $\tilde{a}^1\Delta$, $\tilde{b}^1\Sigma^+$, $\tilde{A}^3\Pi$, and $\tilde{c}^1\Pi$, for NCN (the centrosymmetric isomer of CN_2), the $\tilde{X}^3\Sigma_g^-$ state, and for c-CN_2 (the cyclic isomer of CN_2), its $\tilde{X}^1A_1$ state. The same symmetries, save the $\tilde{c}^1\Pi$, have been examined for CPP, PCP, and c-CP_2, respectively. Our results are summarized below.

(i) For all linear symmetries examined, we have constructed fully optimized MRCI, and in certain cases RCCSD(T), potential energy profiles ("cuts" through the corresponding potential surfaces) of C + X_2 or CX + X, X = N or P, in an effort to follow the (valence) electronic distributions upon the bonding process.

(ii) For the $\tilde{X}^3\Sigma^-$ state of CNN in particular, our calculations indicate that its electronic structure is best described by the conventional formula $\dot{C}{=}N_{(a)}{=}\dot{N}_{(b)}$, i.e., with the triplet-coupled electrons located on the C and the $N_{(b)}$ atoms and two double bonds, as contrasted to the $\tilde{X}^3\Sigma^-$ state of CCO, $\dot{C} - C \equiv O$, with the triplet-coupled electrons localized on the first C atom and with a single and a triple bond. Interestingly enough, the PEPs of both molecules, $CNN(\tilde{X}^3\Sigma^-)$ and $CCO(\tilde{X}^3\Sigma^-)$, are well described at the single reference RCCSD(T) level. This is obvious for the latter but not for the former.

(iii) The construction of MRCI/a5Z PEPs of the first five states of CNN shows clearly their energetic behavior with respect to the asymptotic products $C(^3P)$ + $N_2(X^1\Sigma_g^+)$ and $C(^1D)$ + $N_2(X^1\Sigma_g^+)$, which reveals their bonding complexity, and it is in agreement with certain experimental data.

(iv) For the first time, an effort was made to better understand the bonding and energetics of the first

DOI: 10.1021/acs.jpca.9b09084
J. Phys. Chem. A 2019, 123, 10290−10302

excited triplet $\tilde{A}^3\Pi$ through the construction of the first four PEPs of $^3\Pi$ symmetry at the CASSCF/a5Z level.

(v) With the exceptions of the fundamental vibrational frequencies ω_1, ω_2, and ω_3, which are in fair agreement with the experiment, all our numerical results on CNN are in excellent agreement with existing experimental numbers and with previous theoretical results obtained at a level of theory similar to the present. We refer to the states $\tilde{X}^3\Sigma^-$, $\tilde{a}^1\Delta$, and $\tilde{A}^3\Pi$. It should be stressed that all five states have been examined at a uniform high level of theory, while certain properties like dipole moments ($\tilde{a}^1\Delta$, $\tilde{b}^1\Sigma^+$, $\tilde{c}^1\Pi$) and binding energies ($\tilde{a}^1\Delta$, $\tilde{b}^1\Sigma^+$, $\tilde{A}^3\Pi$, $\tilde{c}^1\Pi$) are reported for the first time at this level of theory and could be considered as definitive.

(vi) Concerning the centrosymmetrical isomer of CN_2, NCN, we have only studied its ground state, $\tilde{X}^3\Sigma_g^-$. Its bonding has been clarified, while its calculated geometry and binding energy with respect to $N(^4S)$ + $CN(X\ ^2\Sigma^+)$ are in excellent agreement with the experiment. On the triplet surface, the $NCN(\tilde{X}^3\Sigma_g^-)$ isomer is more stable than $CNN(\tilde{X}^3\Sigma^-)$ by 48 mE_h (=30.1 kcal/mol) at the MRCI or RCCSD(T)/a5Z levels of theory. The isomerization process $CNN(\tilde{X}^3\Sigma^-) \rightarrow NCN(\tilde{X}^3\Sigma_g^-)$ on the triplet C_s surface through the ∠NCN angle from 180.0 (CNN) to 0.0° (NCN) amounts to a barrier of about 30 kcal/mol at the CASSCF/a5Z level.

(vii) The stability of the cyclic isomer of CN_2, c-CN_2 (cyclic "carbene"), its symmetry being $\tilde{X}^1A_1$, was confirmed at the RCCSD(T)/a5Z level. Its electronic structure is similar to that of cyclopropene carbene, $C(CH)_2(^1A_1)$. Its geometrical structure is very close to previous theoretical calculations at the CCSD(T)/TZ2P level, but its dipole moment μ_e = 0.55 D and dissociation energy with respect to $C(^3P)$ + $N_2(X^1\Sigma_g^+)$ $D_0°$ = 31.3 kcal/mol have been calculated for the first time.

(viii) The PEPs $^3\Sigma^-$, $^1\Delta$, $^1\Sigma^+$, and $^3\Pi$ of the phosphorous analogue of CNN, CPP, show a striking similarity with the corresponding PEPs of CNN; however, only the $^3\Pi$ symmetry is a stationary state. Symmetries $^3\Sigma^-$, $^1\Delta$, and $^1\Sigma^+$ have one imaginary frequency, the bending one $\omega_2(\pi)$. Hence, the ground state of CPP is $\tilde{X}^3\Pi$ and bound with respect to $C(^3P)$ + $P_2(X^1\Sigma_g^+)$ by 7.3 kcal/mol at the RCCSD(T)/a5Z level. The corresponding C−NN value is −39.3 kcal/mol.

(ix) The CPP species on the triplet C_s surface slips barrierlessly to its centrosymmetric isomer $PCP(\tilde{X}^3\Sigma_g^-)$ some 107 kcal/mol lower at the CASSCF/a5Z level. It should be stressed here that for the first time high level MRCI and coupled-cluster results clarified that the previous experimental results on $\Delta_f H$ of CP_2 concerned the PCP $\tilde{X}^3\Sigma_g^-$ isomer.

(x) Finally, the cyclic isomer of CP_2, c-CP_2, was studied for the first time at the RCCSD(T)/a5Z level. It is a singlet of $^1A_1$ symmetry, its electronic structure being similar to that of the isovalent c-CN_2 and with $D_0°$ = 43.2 kcal/mol with respect to $C(^3P)$ + $P_2(X^1\Sigma_g^+)$.

It is hoped that the present study will motivate further experimental and theoretical studies on these unusual and interesting systems.

AUTHOR INFORMATION

Corresponding Authors

*E-mail: papakondylis@chem.uoa.gr (A.P.).
*E-mail: mavridis@chem.uoa.gr (A.M.).

ORCID

Aristotle Papakondylis: 0000-0003-1534-2380

Notes

The authors declare no competing financial interest.

REFERENCES

(1) Robinson, G. W.; McCarthy, M., Jr. The Production and Subsequent Photolysis of Transient Products from the Photodecomposition of Diazomethane at 4.2 °K. *J. Am. Chem. Soc.* **1960**, *82*, 1859−1864.
(2) Goldfarb, T. D.; Pimentel, G. C. Spectroscopic Study of the Photolysis of Diazomethane in Solid Nitrogen. *J. Am. Chem. Soc.* **1960**, *82*, 1865−1868.
(3) Wasserman, E.; Barash, L.; Yager, W. A. The Electron Paramagnetic Resonance of Triplet CNN, NCN, and NCCCN. *J. Am. Chem. Soc.* **1965**, *87*, 2075−2076.
(4) Bondybey, V. E.; English, J. H. W. Spectroscopy and Vibrational Relaxation of CNN in Rare Gas Solids. *J. Chem. Phys.* **1977**, *67*, 664−668.
(5) Wilkerson, J. L.; Guillory, W. A. Laser-Induced Temporal and Wavelength Resolved Spectroscopy of the $^3\Pi$-$^3\Sigma^-$ System of Matrix-Isolated CNN. *J. Mol. Spectrosc.* **1977**, *66*, 188−191.
(6) Thomson, C. Electronic Structure of Unstable Intermediates. II. The Electronic Structure of NNC, NCN, NCC, and CNC. *J. Chem. Phys.* **1973**, *58*, 841−843.
(7) Moll, N. G.; Thomson, W. E. Reaction of Carbon Atoms with N_2, H_2, and D_2 at 4.2 °K. *J. Chem. Phys.* **1966**, *44*, 2684−2686.
(8) Milligan, D. E.; Jacox, M. E. Matrix-Isolation Study of the Infrared and Ultraviolet Spectra of the Free Radical CNN. *J. Chem. Phys.* **1966**, *44*, 2850−2856.
(9) DeKock, R. L.; Weltner, W., Jr. C_2O, CN_2, and C_3O Molecules. *J. Am. Chem. Soc.* **1971**, *93*, 7106−7107.
(10) Jacox, M. E. Matrix Isolation Study of the Reaction of Carbon Atoms with Molecular Nitrogen. Electronic Transitions of the CNN Free Radical in the 2600- to 1900-Å Spectral Region. *J. Mol. Spectrosc.* **1978**, *72*, 26−35.
(11) Curtis, M. C.; Levick, A. P.; Sarre, P. J. Laser-Induced-Fluorescence Spectrum of the CNN Molecule. *Laser Chem.* **1988**, *9*, 359−368.
(12) Wurfel, B. E.; Thoma, A.; Sclachta, R.; Bondybey, V. E. Laser Induced Fluorescence of CNN in an Ar Matrix. *Chem. Phys. Lett.* **1992**, *190*, 119−123.
(13) Clifford, E. P.; Wenthold, P. G.; Lineberger, W. C.; Petersson, G. A.; Broadus, K. M.; Kass, S. R.; Kato, S.; DePuy, C. H.; Bierbaum, V. M.; Ellison, G. B. Properties of Diazocarbene [CNN] and the Diazomethyl Radical [HCNN] via Ion Chemistry and Spectroscopy. *J. Phys. Chem. A* **1998**, *102*, 7100−7112.
(14) Bise, R. T.; Hoops, A. A.; Choi, H.; Neumark, D. M. Photodissociation Dynamics of the CNN Free Radical. *J. Chem. Phys.* **2000**, *113*, 4179−4189.
(15) Hickson, K. M.; Loison, J.-C.; Lique, F.; Kłos, J. An Experimental and Theoretical Investigation of the $C(^1D)$ + $N_2 \rightarrow$ $C(^3P)$ + N_2 Quenching Reaction at Low Temperature. *J. Phys. Chem. A* **2016**, *120*, 2504−2513.
(16) DeKock, R. L.; Grev, R. S.; Schaefer, H. F., III The Valence Isoelectronic Molecules CCO, CNN, SiCO, and SiNN in Their Triplet Ground States: Theoretical Predictions of Structures and Infrared Spectra. *J. Chem. Phys.* **1988**, *89*, 3016−3027.
(17) Cai, Z.-L.; Sha, G.-H.; Zhang, C.-H.; Huang, M.-B. CI Studies of Four Low-Lying Electronic States of the CNN Radical. *J. Mol. Struct.: THEOCHEM* **1992**, *253*, 303−309.

DOI: 10.1021/acs.jpca.9b09084
J. Phys. Chem. A 2019, 123, 10290−10302

(18) Martin, J. M. L.; Taylor, P. R.; François, J. P.; Gijbels, R. Ab Initio Study of the Spectroscopy and Thermochemistry of the C_2N and CN_2 Molecules. *Chem. Phys. Lett.* **1994**, *226*, 475−485.
(19) Sutar, H. U.; Huang, M.-B.; Engels, B. A Multireference Configuration Interaction Study of the Hyperfine Structure of the Molecules CCO, CNN, and NCN in Their Triplet Ground States. *J. Chem. Phys.* **1994**, *101*, 7686−7691.
(20) Pd, R.; Chandra, P. J. Ground and Valence Excited States of C_2N and CN_2 Transients: Ab Initio Geometries, Electronic Structures, and Molecular Properties. *J. Chem. Phys.* **2001**, *114*, 1589−1600.
(21) Yamaguchi, Y.; Schaefer, H. F. The Diazocarbene (CNN) Molecule: Characterization of the $\tilde{X}^3\Sigma^-$ and $\tilde{A}^3\Pi$ Electronic States. *J. Chem. Phys.* **2004**, *120*, 9536−9546.
(22) Melnikov, V. V.; Jensen, P. Potential Energy Surface and Spectroscopic Parameters of $\tilde{X}^3\Sigma^-$ CNN. *Chem. Phys. Lett.* **2004**, *394*, 171−175.
(23) Carter, S.; Handy, N. C.; Yamaguchi, Y.; Turney, J. M.; Schaefer, H. F., III Vibrational Energy Levels for the Electronic Ground State of the Diazocarbene (CNN) Molecule. *Mol. Phys.* **2008**, *106*, 357−365.
(24) Alves, T. V.; Aoto, Y. A.; Ornellas, F. R. Structural and Spectroscopic Properties of the Diazocarbene Radical (CNN) and Its Ions CNN^+ and CNN^-: A High-Level Theoretical Investigation. *Mol. Phys.* **2010**, *108*, 2061−2071.
(25) An, F.; Han, S.; Hu, X.; Xie, D.; Guo, H. First-Principles Dynamics of Collisional Intersystem Crossing: Resonance Quenching of $C(^1D)$ by N_2. *Phys. Chem. Chem. Phys.* **2019**, *21*, 8645−8653.
(26) Jacox, M. E. Vibrational and Electronic Energy Levels of Polyatomic Transient Molecules. Supplement B. *J. Phys. Chem. Ref. Data* **2003**, *32*, 1−441.
(27) Dunning, T. H., Jr. Gaussian Basis Sets for Use in Correlated Molecular Calculations. I. The Atoms Boron through Neon and Hydrogen. *J. Chem. Phys.* **1989**, *90*, 1007−1023.
(28) Smoes, S.; Myers, C. E.; Drowart, J. Determination of the Atomization Energies of CP, C_2P, CP_2, and C_2P_2 by High Temperature Knudsen Cell Mass Spectrometry. *Chem. Phys. Lett.* **1971**, *8*, 10−12.
(29) Kordis, J.; Gingerich, K. A. Gaseous Phosphorous Compounds. IX. Mass Spectrometric Studies of Equilibria in the Carbon-Phosphorous System. *J. Chem. Phys.* **1973**, *58*, 5058−5066.
(30) Huber, K. P.; Herzberg, G. *Molecular Spectra and Molecular Structure. IV. Constants of Diatomic Molecules*; Van Nostrand Reinhold Company: NY, 1979.
(31) Brown, S. T.; Yamaguchi, Y.; Schaefer, H. F. $\tilde{X}^3\Sigma^-$ and $\tilde{A}^3\Pi$ Electronic States of Ketenylidene (CCO): Analysis of the Renner Effect in the Upper State. *J. Phys. Chem. A* **2000**, *104*, 3603−3612.
(32) Kendall, R. A.; Dunning, T. H., Jr.; Harrison, R. J. Electron Affinities of the First Row Atoms Revisited. Systematic Basis Sets and Wave Functions. *J. Chem. Phys.* **1992**, *96*, 6796−6806.
(33) Woon, D. E.; Dunning, T. H., Jr. Gaussian Basis Sets for Use in Correlated Molecular Calculations. III. The Atoms Aluminum through Argon. *J. Chem. Phys.* **1993**, *98*, 1358−1371.
(34) Raghavachari, K.; Trucks, G. W.; Pople, J. A.; Head-Gordon, M. A Fifth Order Perturbation Comparison of Electron Correlation Theories. *Chem. Phys. Lett.* **1989**, *157*, 479−483.
(35) Watts, J. D.; Gauss, J.; Bartlett, R. J. Coupled-Cluster Methods with Noniterative Triple Excitations for Restricted Open-Shell Hartree-Fock and Other General Single Determinant Reference Functions. Energies and Analytical Gradients. *J. Chem. Phys.* **1993**, *98*, 8718−8733.
(36) Knowles, P. J.; Hampel, C.; Werner, H.-J. Coupled-Cluster Theory for High Spin Open Shell Reference Wave Functions. *J. Chem. Phys.* **1993**, *99*, 5219−5227.
(37) Werner, H.-J.; Knowles, P. J. An Efficient Internally Contracted Multiconfiguration−Reference Configuration Interaction Method. *J. Chem. Phys.* **1988**, *89*, 5803−5814.
(38) Knowles, P. J.; Werner, H.-J. An Efficient Method for the Evaluation of Coupling Coefficients in Configuration Interaction Calculations. *Chem. Phys. Lett.* **1988**, *145*, 514−522.
(39) Langhoff, S. R.; Davidson, E. R. Configuration Interaction Calculations on the Nitrogen Molecule. *Int. J. Quantum Chem.* **1974**, *8*, 61−72.
(40) Davidson, E. R.; Silver, D. W. Size Consistency in the Dilute Helium Gas Electronic Structure. *Chem. Phys. Lett.* **1977**, *52*, 403−406.
(41) Werner, H.-J.; Knowles, P. J.; Knizia, G.; Manby, F. R.; Schütz, M.; Celani, P.; Gyoffry, W.; Korona, T.; Lindh, R.; Mitrushenkov, A. et al. *MOLPRO*, version 2015.1, 2015. http://www.molpro.net.
(42) Beaton, S. A.; Yoshiro, I.; Brown, J. M. Laser Excitation Spectroscopy of the $\tilde{A}^3\Pi_u - \tilde{X}^3\Sigma_g^-$ Transition of the NCN Radical. *J. Mol. Spectrosc.* **1996**, *178*, 99−107.
(43) Bise, R. T.; Choi, H.; Neumark, D. M. Photodissociation Dynamics of the Singlet and Triplet States of the NCN Radical. *J. Chem. Phys.* **1999**, *111*, 4923−4932.
(44) Choi, H.; Mordaunt, D. H.; Bise, R. T.; Taylor, T. R.; Neumark, D. M. Photodissociation of Triplet and Singlet States of the CCO Radical. *J. Chem. Phys.* **1998**, *108*, 4070−4078.
(45) Kramida, A.; Ralchenko, Y.; Reader, J.; NIST ASD Team. *NIST Atomic Spectra Database*, version 5.7.1 (accessed Oct 22, 2019). http://physics.nist.gov/asd.
(46) Kalemos, A.; Ariyarathna, I. R.; Khan, S. N.; Miliordos, E.; Mavridis, A. Hypervalency and the Chemical Bond. *Comput. Theor. Chem.* **2019**, *1153*, 65−74.
(47) Clifford, E. P.; Weinhold, P. G.; Lineberger, W. G.; Petterson, G. A.; Ellison, G. B. Photoelectron Spectroscopy of the NCN^- and $HNCN^-$ Ions. *J. Phys. Chem. A* **1997**, *101*, 4338−4345.
(48) Hanzlová, E.; Navrátil, R.; Čejka, J.; Böhm, S.; Martinů, T. Evidence for the Cyclic CN_2 Carbene in Solution. *Org. Lett.* **2014**, *16*, 852−855.
(49) Hanzlová, E.; Váňa, J.; Shaffer, C. J.; Roithová, J.; Martinů, T. Evidence for the Cyclic CN_2 Carbene in the Gas Phase. *Org. Lett.* **2014**, *16*, 5482−5485.
(50) Jursic, B. S. High Level Ab Initio Study of Singlet and Triplet Cyclopropene and Diazocyclopropene Carbenes Stability in Comparison with Stability of Singlet and Triplet Cyclopropenyl Cation and Anion. *J. Mol. Struct.: THEOCHEM* **1999**, *491*, 33−40.
(51) Kalemos, A.; Mavridis, A.; Metropoulos, A. An Accurate Description of the Ground and Excited States of CH. *J. Chem. Phys.* **1999**, *111*, 9536−9548.
(52) Chase, M. W., Jr. NIST-JANAF Tables. *J. Phys. Chem. Ref. Data, Monogr. 9* **1998**, 1−1951.
(53) Fleming, P. E.; Lee, E. P. F.; Wright, T. G. The Ionization Energy and ΔH_f (0 K) of CP, PCP and PCCP. *Chem. Phys. Lett.* **2000**, *332*, 199−207.

DOI: 10.1021/acs.jpca.9b09084
J. Phys. Chem. A 2019, 123, 10290−10302